

Comparison of Physical Connectivity Particle Tracking Models in the Flemish Cap Region

Shuangqiang Wang, Zeliang Wang, Camille Lirette, Andrew J. Davies,
and Ellen. L. Kenchington

Ocean and Ecosystem Sciences Division
Maritimes Region

Fisheries and Oceans Canada
Bedford Institute of Oceanography
PO Box 1006
Dartmouth, Nova Scotia
Canada B2Y 4A2

2019

**Canadian Technical Report of
Fisheries and Aquatic Sciences 3353**



Canadian Technical Report of Fisheries and Aquatic Sciences

Technical reports contain scientific and technical information that contributes to existing knowledge but which is not normally appropriate for primary literature. Technical reports are directed primarily toward a worldwide audience and have an international distribution. No restriction is placed on subject matter and the series reflects the broad interests and policies of Fisheries and Oceans Canada, namely, fisheries and aquatic sciences.

Technical reports may be cited as full publications. The correct citation appears above the abstract of each report. Each report is abstracted in the data base *Aquatic Sciences and Fisheries Abstracts*.

Technical reports are produced regionally but are numbered nationally. Requests for individual reports will be filled by the issuing establishment listed on the front cover and title page.

Numbers 1-456 in this series were issued as Technical Reports of the Fisheries Research Board of Canada. Numbers 457-714 were issued as Department of the Environment, Fisheries and Marine Service, Research and Development Directorate Technical Reports. Numbers 715-924 were issued as Department of Fisheries and Environment, Fisheries and Marine Service Technical Reports. The current series name was changed with report number 925.

Rapport technique canadien des sciences halieutiques et aquatiques

Les rapports techniques contiennent des renseignements scientifiques et techniques qui constituent une contribution aux connaissances actuelles, mais qui ne sont pas normalement appropriés pour la publication dans un journal scientifique. Les rapports techniques sont destinés essentiellement à un public international et ils sont distribués à cet échelon. Il n'y a aucune restriction quant au sujet; de fait, la série reflète la vaste gamme des intérêts et des politiques de Pêches et Océans Canada, c'est-à-dire les sciences halieutiques et aquatiques.

Les rapports techniques peuvent être cités comme des publications à part entière. Le titre exact figure au-dessus du résumé de chaque rapport. Les rapports techniques sont résumés dans la base de données *Résumés des sciences aquatiques et halieutiques*.

Les rapports techniques sont produits à l'échelon régional, mais numérotés à l'échelon national. Les demandes de rapports seront satisfaites par l'établissement auteur dont le nom figure sur la couverture et la page du titre.

Les numéros 1 à 456 de cette série ont été publiés à titre de Rapports techniques de l'Office des recherches sur les pêcheries du Canada. Les numéros 457 à 714 sont parus à titre de Rapports techniques de la Direction générale de la recherche et du développement, Service des pêches et de la mer, ministère de l'Environnement. Les numéros 715 à 924 ont été publiés à titre de Rapports techniques du Service des pêches et de la mer, ministère des Pêches et de l'Environnement. Le nom actuel de la série a été établi lors de la parution du numéro 925.

Canadian Technical Report of
Fisheries and Aquatic Sciences 3353

2019

Comparison of Physical Connectivity Particle Tracking Models in the Flemish Cap Region

by

Shuangqiang Wang, Zeliang Wang, Camille Lirette, Andrew J. Davies¹,

and

Ellen L. Kenchington

Ocean and Ecosystem Sciences Division
Maritimes Region
Fisheries and Oceans Canada
Bedford Institute of Oceanography
Dartmouth, N.S.
Canada B2Y 4A2

¹ University of Rhode Island,
Department of Biological Sciences,
Woodward Hall,
9 East Alumni Avenue,
Kingston, RI 02881, USA

© Her Majesty the Queen in Right of Canada, 2019.
Cat. No. Fs97-6/3353E-PDF ISBN 978-0-660-33600-8 ISSN 1488-5379

Correct citation for this publication:

Wang, S., Wang, Z., Lirette, C., Davies, A. and Kenchington, E. 2019. Comparison of Physical Connectivity Particle Tracking Models in the Flemish Cap Region. Can. Tech. Rep. Fish. Aquat. Sci. 3353: v + 39 p.

TABLE OF CONTENTS

ABSTRACT	iv
RÉSUMÉ	v
INTRODUCTION	1
METHODOLOGY	3
PARCELS FRAMEWORK	3
DETERMINATION OF OPTIMAL PARAMETER VALUES.....	3
<u>Number of Particles</u>	4
<u>Time Step</u>	4
<u>Random Walk</u>	4
<u>Number of Particles with Random Walk Applied</u>	5
SIMULATION EXPERIMENTS	5
<u>Impacts of Random Walk on Connectivity</u>	5
<u>Identification of Potential Source Populations</u>	6
<u>Connectivity among Closed Areas</u>	7
COMPARISON OF CONNECTIONS PRODUCED WITH WEBDROGUE AND PARCELS	
.....	7
RESULTS	7
OPTIMIZATION OF PARAMETERS	7
<u>Number of Particles to Seed</u>	7
<u>Time Step</u>	9
<u>Random Walk</u>	10
<u>Number of Particles with Random Walk Applied</u>	18
SIMULATION EXPERIMENTS	20
<u>Impacts of Random Walk on Connectivity</u>	20
<u>Identification of Potential Source Populations</u>	22
<u>Connectivity Among Closed Areas</u>	24
COMPARISON OF CONNECTIONS PRODUCED WITH WEBDROGUE AND PARCELS	
.....	32
DISCUSSION	34
ACKNOWLEDGEMENTS	36
REFERENCES	36
APPENDIX 1. CORRECTING PARTICLE TRAJECTORIES EXTENDING ONTO LAND	
THROUGH RANDOM WALK IN PARCELS	39

ABSTRACT

Wang, S., Wang, Z., Lirette, C., Davies, A. and Kenchington, E. 2019. Comparison of Physical Connectivity Particle Tracking Models in the Flemish Cap Region. Can. Tech. Rep. Fish. Aquat. Sci. 3353: v + 39 p.

Lagrangian particle tracking models are considered an important tool for assessing connectivity in the deep sea. A number of user interfaces are available to assess oceanic structural connectivity. These use currents produced by state-of-the-art ocean models, and can be used to run forward/hindcast simulations, habitat connectivity calculations, comparison of physical circulation models, etc. We compared simulation outputs from two particle tracking packages, WebDrogue v.0.7 and the Parcels framework version 2.1, the former having been previously published in a study investigating connectivity patterns among closed areas in the NAFO Regulatory Area. We further tested a combination of parameters used by Parcels (number of particles, particle spacing, time step, random walk) to determine optimal values for future applications. Parcels identified more connectivity than WebDrogue with differences attributed to higher current velocities in the underlying ocean model, although drift pathways were generally similar in both.

RÉSUMÉ

Wang, S., Wang, Z., Lirette, C., Davies, A. and Kenchington, E. 2019. Comparison of Physical Connectivity Particle Tracking Models in the Flemish Cap Region. Can. Tech. Rep. Fish. Aquat. Sci. 3353: v + 39 p.

On considère que les modèles Lagrangien de suivi de particules sont un outil important pour évaluer la connectivité en haute mer. Il existe un certain nombre d'interfaces utilisateur permettant d'évaluer la connectivité structurelle des océans. Ces interfaces, qui utilisent les courants issus de modèles océaniques de pointe, peuvent entre autres servir à effectuer des simulations prospectives ou rétrospectives, à faire des calculs liés à la connectivité de l'habitat ainsi qu'à comparer des modèles de circulation physique. Dans le cadre de la présente étude, nous avons comparé les résultats de simulation issus de deux interfaces de suivi de particules, soit la version 0.7 de WebDrogue et la version 2.1 de Parcels. Les résultats de simulation issus de WebDrogue ont déjà été publiés dans le cadre d'une étude sur les tendances de connectivité au sein de zones fermées situées au sein de la zone réglementée par l'OPANO. Nous avons donc testé une combinaison de paramètres utilisés par Parcels (nombre de particules, espace entre les particules, intervalle de temps, marche aléatoire) afin de déterminer les valeurs optimales pour des applications futures. Les résultats montrent que la connectivité calculée par Parcels est plus élevée que celle calculée par WebDrogue; les différences sont attribuables à des vitesses de courants plus élevées dans le modèle océanique sous-jacent, même si les trajectoires de dérive sont généralement similaires pour les deux interfaces.

INTRODUCTION

Conservation of vulnerable benthic organisms, which have lifecycles that include planktonic larvae, may require management of anthropogenic impacts not only where adult organisms form rich growths but also in up-stream sources of future recruitment. Lagrangian particle tracking (LPT) models are valuable tools for conceptualizing and quantifying connectivity between larval sources and settlement in the deep sea (e.g., Adams et al. 2011, Breusing et al. 2016, Xu et al. 2018, Bracco et al. 2019, Kenchington et al. 2019, Zeng et al. 2019). In such models, virtual particles are advected by flow fields derived from numerical ocean models (Lange and Seville 2017). In some models, virtual behaviour can also be added to the particles so that they mimic active larval movements, rather than act as passive drifters (e.g., chemical pollutants). A number of user interfaces are available to assess oceanic connectivity using LPT models. These combine complex individual-level models of particles with a state-of-the-art 3-D oceanographic model of the physics, and can be used to run forward/hindcast simulations, habitat connectivity calculations, comparison of physical circulation models, etc.

The Northwest Atlantic Fisheries Organization (NAFO) has closed 14 areas in the high seas (NAFO Regulatory Area; NRA) of the northwest Atlantic to bottom trawling to protect vulnerable marine ecosystems (Figure 1), and particularly the deep-sea sponges, sea pens and gorgonian corals that are found there. Kenchington et al. (2019) evaluated connectivity among those closures using a LPT model, the “WebDrogue Drift Prediction Model v.0.7” coupled with the “Southern Labrador, Newfoundland Shelf” data set (<http://www.bio.gc.ca/science/research-recherche/ocean/WebDrogue/slns-tnls-en.php>) to compute passive-particle drift trajectories. WebDrogue has a number of limitations when it comes to application to the NRA. Particle tracking is limited to relatively shallow depth zones using vertical averages of the velocity fields for each depth interval: 0-5 m (surface), 25-35 m (25 m), and 95-105 m (100 m). To examine drift trajectories at greater depths (1000 m and the seabed), Kenchington et al. (2019) extrapolated the WebDrogue results from 100 m to greater depths with the aid of the eddy-resolving “Bedford Institute of Oceanography North Atlantic Model” (BNAM; Wang et al. 2016).

A number of alternative LPT models are available which allow for calculation of horizontal velocities at greater depths than those available in WebDrogue, including “Ariane” (Blanke and Raynaud 1997), “TRACMASS” (Döös et al. 2017) and the “Parcels framework” (<http://www.oceanparcels.org>; Lange and van Sebille 2017, Delandmeter and van Sebille 2019). We have selected Parcels version 2.1, which was developed to optimize computational efficiency and scalability, for further exploration of the connectivity among NAFO’s 14 closed areas.

WebDrogue and Parcels use different ocean models. The ocean circulation model underlying the tracking algorithm in WebDrogue is the “Dartmouth Finite Element Model” or “Quoddy”, a finite-element computer simulation program for coastal ocean circulation modeling (Lynch and Werner 1991). Details of the computation of the circulation components have been provided by Hannah et

al. (2000) and those of regional data sources by Han et al. (2008). The particle tracking algorithm used in WebDrogue is based on the “DROG3-D” program (Werner et al. 1993; Blanton 1995).

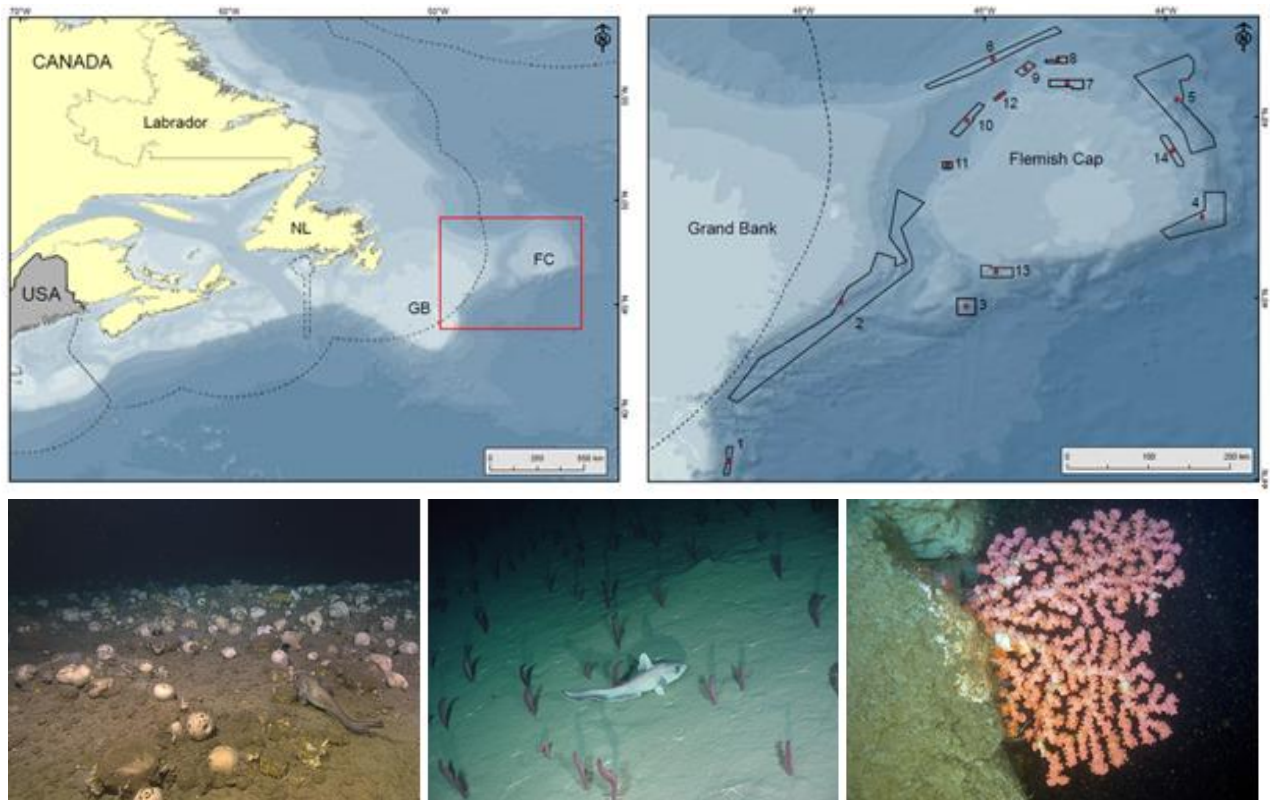


Figure 1. Upper row: Location of the 14 areas closed to protect coral and sponge vulnerable marine ecosystems in the NAFO Regulatory Area. Dashed lines represent the exclusive economic zones. Red box shows area illustrated in right panel. Lower row (left to right): Images of deep-sea sponges, sea pens and large gorgonian corals protected by the closures.

Parcels was used in conjunction with the eddy-resolving Bedford Institute of Oceanography North Atlantic model (BNAM) (Wang et al. 2016, Wang et al. 2019), which uses the NEMO 2.3 (Nucleus for European Modelling of the Ocean) model engine. NEMO is a structured, z-level grid ocean model (Madec et al. 2016).

In preparation for forthcoming studies of 3-D connectivity, we here repeat the principal LPT analyses presented by Kenchington et al. (2019) but using the Parcels framework. We compare the outputs from those analyses with both the results previously derived using WebDrogue and the former extrapolations to depths greater than 100 m. We precede those analyses with determination of the optimal parameter sets for our application of Parcels.

METHODOLOGY

PARCELS FRAMEWORK

Kenchington et al. (2019) presented WebDrogue results for each of four two-month seasons (Winter: January, February; Spring: April, May; Summer: July, August; and Autumn: October, November) and for horizontal advection at depths of 0-5 m (“surface”) and 95-105 m (“100 m”), with all velocity fields vertically averaged across each depth interval. Virtual Lagrangian particles were released at each depth and in each of the 14 closed areas. Their drifts were modelled over durations of 2 weeks, 1 month and 3 months (periods corresponding to the expected planktonic larval lives of the benthic species that, by management intent, are protected by the closures) in both forecast and hindcast modes to identify dispersal kernels. That modelling was repeated here but using Parcels framework version 2.1 (<http://www.oceanparcels.org>; Lange and van Sebille 2017, Delandmeter and van Sebille 2019) using the fourth-order Runge-Kutta method (Runge-Kutta 4 default option in Parcels) as the integration scheme. For comparison with the WebDrogue results of Kenchington et al. (2019), only 2-D trajectories were calculated.

In this study, Parcels drew climatological monthly-mean currents from the BNAM oceanographic model (Wang et al. 2016, Wang et al. 2019, Brickman et al. 2015, Brickman et al. 2018) over the period 1990-2015. BNAM is an eddy-resolving North Atlantic Ocean model with a nominal resolution of $1/12^\circ$ (approx. 8 km at the Equator). It is based on “Nucleus for European Modelling of the Ocean” (NEMO) 2.3. BNAM has a maximum of 50 depth levels, with thicknesses increasing from 1 m at the surface to 200 m at a depth of 1250 m and reaching a maximum of 460 m at the bottom of the deep basins.

Particles were deleted if they reached the boundary of a spatial domain delineated by the marine area bounded by the 31.4° and 67.3° W meridians and by the 34.5° and 58.6° N parallels of latitude. Trajectories were prevented from extending onto land (which can occur with Parcels 2.1 if the time step is large enough that particles step over multiple grid cells in one increment or if random walk is implemented) by initializing the diffusivity as zero in land areas (Appendix 1).

DETERMINATION OF OPTIMAL PARAMETER VALUES

Parcels requires user input of the number of particles, which also determines the initial particle spacing, and of the time step used in calculating virtual trajectories. Alternative values were evaluated iteratively to determine optimal values that minimized computational time without introducing bias. We also tested the sensitivity of analytical outputs to the values selected for horizontal diffusivity, and optimized particle number for a horizontal diffusivity of $100 \text{ m}^2 \text{ s}^{-1}$.

Number of Particles

The sensitivity of Parcels output to the release of different numbers of virtual particles was first assessed through calculation of trajectories, without random walk, of simulated particles released within the Closed Areas. Total numbers of particles released in the various scenarios were: 581, 912, 1194, 1636, 2368, 3691, 4560, 5824, 6596, 7608, 10307, 14909, 18404, 23385, 30494, 41479 and 59834, corresponding to a uniform distribution of release sites (within the Closed Areas) at particle-release spacings of 0.05, 0.04, 0.035, 0.03, 0.025, 0.02, 0.018, 0.016, 0.015, 0.014, 0.012, 0.01, 0.009, 0.008, 0.007, 0.006 and 0.005 degrees of latitude and longitude, respectively. The scenarios otherwise followed the forecast models of Kenchington et al. (2019), except that they were only calculated for the winter season.

For each scenario, the number of particles in each cell of a $0.1^\circ \times 0.1^\circ$ grid at the end of each drift duration was counted and transformed into a proportion of the total number of released particles. Pearson correlation coefficients (r) were calculated between the results of scenarios with sequential particle numbers (e.g., 581 vs. 912, 912 vs. 1194 etc.). From inspection of the relationship between correlation and particle number, an optimal number of particles was determined as the minimum number needed to achieve stable outputs. The proportions of particles in each grid cell at the end of each drift duration time were mapped for both the optimal and the maximum number, the maps being compared for each scenario to determine if there was any apparent bias in spatial patterns associated with the selected optimal number of particles.

Time Step

The optimal time step for integrating the trajectories was evaluated using the same approach, with a constant 3691 particles released and hence a particle-release spacing of 0.02° . Time steps of 120, 90, 60, 48, 30, and 12 minutes were used for simulation, and Pearson correlation coefficients (r) were calculated between the results of scenarios with sequential time steps (e.g., 120 vs. 90, 90 vs. 60 etc.).

Random Walk

Introduction of random walk (referred to as Brownian motion in Parcels), into LPTs is an efficient way to both incorporate dispersion and mimic processes which are not resolved or represented in ocean models (Luhar and Rao 1993). It has been extensively used in biophysical modelling of drifts of planktonic larvae and eggs (e.g., Brickman and Smith 2002).

The sensitivity of outputs to various values of the horizontal diffusivity parameter of random walk was evaluated with the number of particles set at 3,691, particle-release spacing at 0.02° and the time step at 60 minutes. The scenarios tested used horizontal diffusivity coefficients of 0, 30, 50, 80, 100, 120, 150, 180 and $200 \text{ m}^2 \text{ s}^{-1}$, the zero value replicating the absence of random walk in the WebDrogue results presented by Kenchington et al. (2019). Rather than calculating correlation coefficients from the outputs of scenarios with sequential diffusivity coefficients, they were calculated between the results of each scenario with finite diffusivity those from the scenario with

no diffusivity (e.g., 0 vs. 30, 0 vs. 50 etc.). Maps were produced for diffusivity-coefficient values of 0, 100 and 200 $\text{m}^2 \text{s}^{-1}$ and compared.

Number of Particles with Random Walk Applied

Optimization of the number of particles was repeated with horizontal diffusivity set to 100 $\text{m}^2 \text{s}^{-1}$ and a time step of 60 min. The same protocols and scenarios were followed as for the initial assessment of particle number.

SIMULATION EXPERIMENTS

Three different simulation experiments were performed using the Parcels framework, each a comparison of an aspect of biophysical connectivity among the closed areas on Flemish Cap performed previously with WebDrogue. Within each experiment, a number of scenarios were run, evaluating different depths and drift durations (Table 1). Selected depths were the surface and 100 m that were modelled by Kenchington et al. (2019), plus 1000 m. The previous study extrapolated model results to that depth, which approximates to the seabed depths in the closed areas (Table 2). Drift durations followed Kenchington et al. (2019), who based them on a review of the life-history characteristics of the coral, sponge and sea pen species that are protected by the closures (Kenchington et al. 2019). All scenarios used annual-average climatological currents from BNAM, 60 min time steps and (except when random walk was turned off) a horizontal diffusivity of 100 $\text{m}^2 \text{s}^{-1}$.

Table 1. Particle-tracking experiments performed with Parcels v.2.1.

Characteristic Examined	Particle Release Depths	Drift Durations
Impacts of random walk	1000 m	2 weeks, 1 month and 3 months
Potential source populations	Surface, 100 m, 1000 m	2 weeks, 1 month and 3 months
Connectivity	Surface, 100 m, 1000 m	2 weeks, 1 month and 3 months

Impacts of Random Walk on Connectivity

The impacts of random walk on connectivity were investigated by comparing the percentage of simulated particles passing over or ending in each closed area with or without inclusion of random walk in the scenario. Based on the results of the parameter optimization, scenarios with random walk used a particle-release spacing of 0.01° . Because the Closed Areas differ in surface area deeper than 1000 m, the number of simulated particles released in each Area varied, while the total was 11,399 (Table 2). The alternative scenarios had zero horizontal diffusivity, to eliminate random walk, and a particle-release spacing of 0.01° .

Table 2. Mean depth of the each of the NAFO closed areas included in the present study and the numbers of virtual particles released within each area for each scenario that used random walk.

Closed Area	Mean Depth (m)	Numbers of Simulated Particles Released with Random Walk	
		Surface and 100 m	1000 m
1	1,516	166	166
2	1,262	6,450	5,334
3	1,431	340	312
4	1,272	1,594	1,088
5	1,776	3,489	3,022
6	1,562	1,173	1,144
7	650	283	0
8	978	113	0
9	992	157	1
10	1,127	377	321
11	1,067	70	11
12	958	41	0
13	666	379	0
14	627	277	0
Total		14,909	11,399

Identification of Potential Source Populations

Possible sources of the larvae that settle in the Closed Areas were identified both by back-tracking simulated particles released within the Areas and forward-tracking of particles released broadly. The scenarios were run with random walk, three drift durations and simulated particles released at three depths (Table 1). Particle-release spacing was uniform and 0.01° throughout.

For back-tracking, particles were only released inside the closed areas, in the numbers given in Table 2. Their positions at the end of each drift duration were binned on a $0.1^\circ \times 0.1^\circ$ grid throughout the model domain and the number in each bin counted. For forward-tracking, 2,559,354 simulated particles were released at each of the surface and 100 m depth, while seabed depths limited the release at 1000 m to 927,621 particles. The release points of particles that followed trajectories which either passed over or ended in a closed area were binned on a $0.1^\circ \times 0.1^\circ$ grid and counted. Maps were constructed using the $0.1^\circ \times 0.1^\circ$ grid.

Connectivity among Closed Areas

Horizontal connectivity among closed areas was assessed at three depths, over three drift durations (Table 1), using 0.01° particle-release spacing. For those simulated particles released within each closed area that passed over another area, the minimum, mean, and maximum times of the transit between each pair of areas were determined. Connectivity was quantified by both arrival time (how long it takes simulated particles from a release area to reach another closed area) and the percentage of particles passing over or ending in another a closed area (Goldsmith et al. 2019). Given the limited pelagic larval durations expected for the coral and sponge species in this area (Kenchington et al. 2019), the sooner that particles reach a particular location, the higher the probability of successful settlement. Kenchington et al. (2019) did not record the number of particles passing over another closed area (they only recorded endpoints).

COMPARISON OF CONNECTIONS PRODUCED WITH WEBDROGUE AND PARCELS

Trajectories modelled using the Parcels framework and BNAM were compared with those generated by Kenchington et al. (2019) using WebDrogue and the Quoddy ocean model. For those comparisons, the scenarios calculated with Parcels were initiated with the same number of simulated particles as used by Kenchington et al. (2019): 50 in each closed area and 700 in total. The calculations were performed for each season. Random walk was not applied under Parcels. The number of connections among closed areas and the areas of retention were compared.

RESULTS

OPTIMIZATION OF PARAMETERS

Number of Particles to Seed

The correlation between proportions of virtual particles in various grid cells, at the end of the drift duration, approached 0.95 when calculated for scenarios in which 2,368 and 3,691 particles were released, for any of the three drift durations or two depths examined (Figure 2). Mapped distributions of the particles at the end of each drift duration showed a high level of congruence between scenarios with those numbers released (e.g., Figure 3). Thus, a release of 3,691 particles, corresponding to a spacing of 0.02° , was sufficient for our subsequent optimization tests.

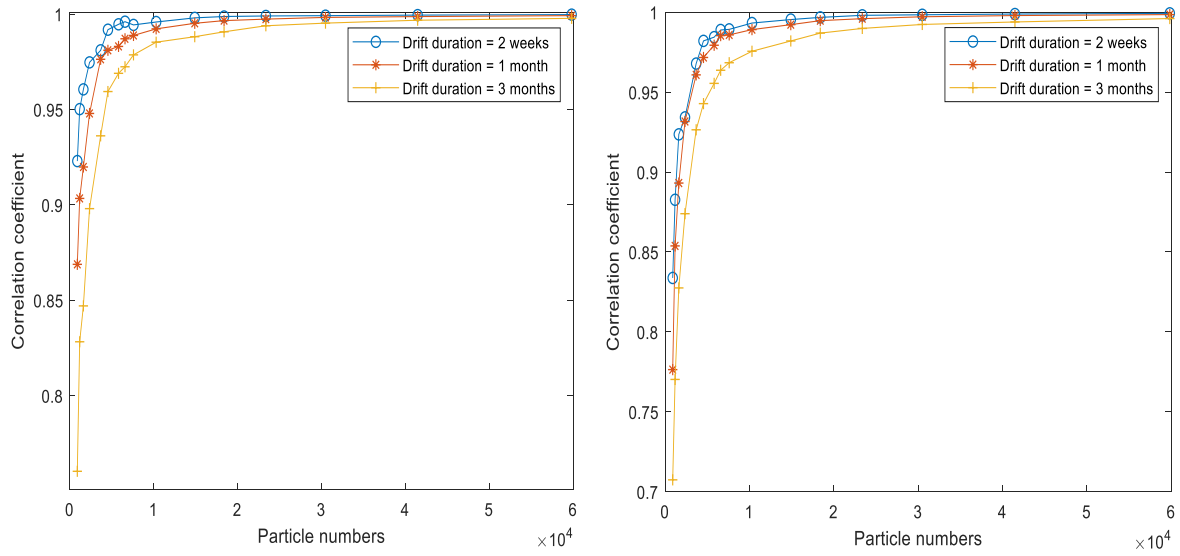


Figure 2. Correlation (r) between proportions of virtual particles in various grid cells, at the end of the drift duration, for sequential pairs of numbers of particles released in winter scenarios at the surface (left) and at a depth of 100 m (right).

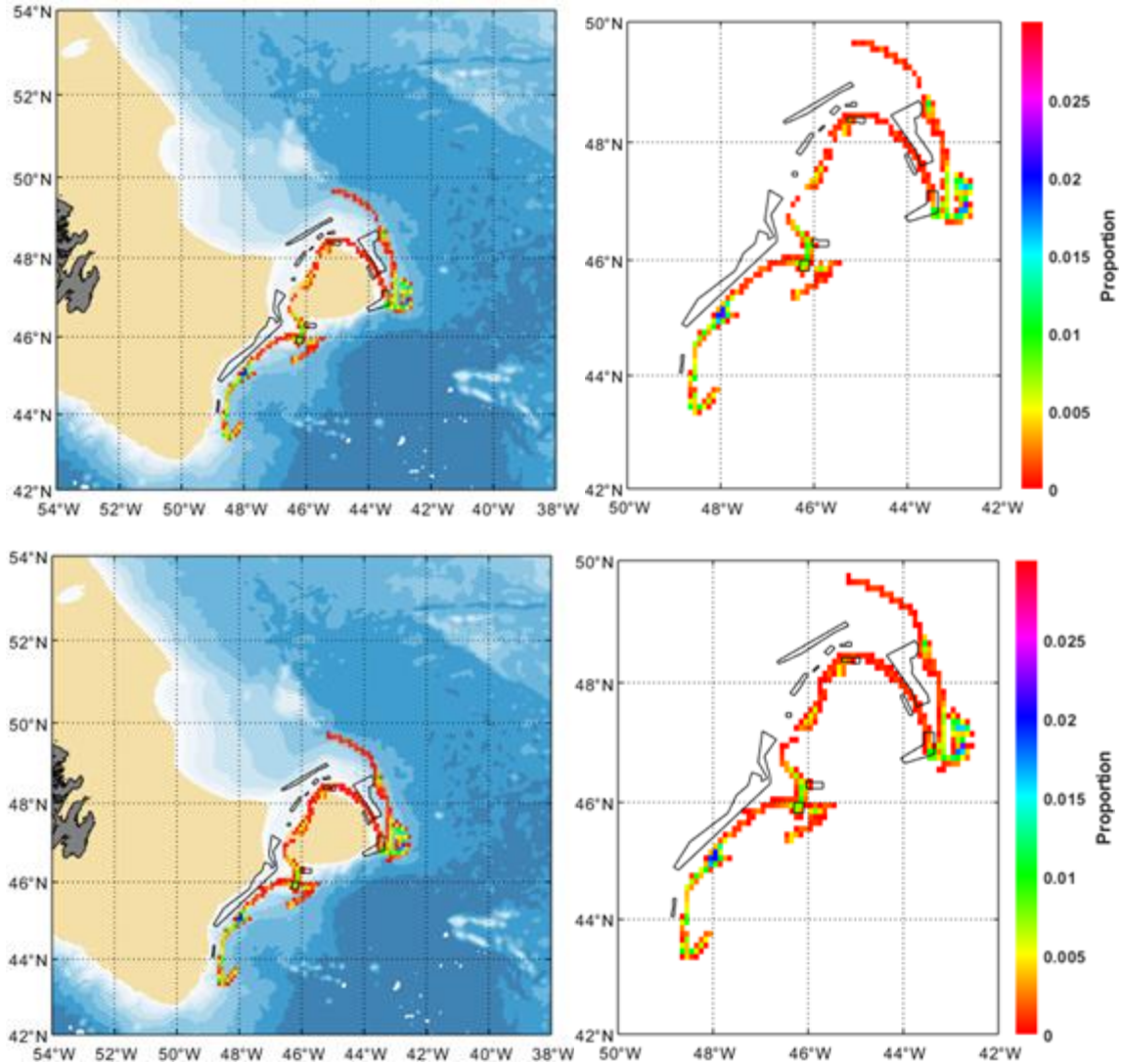


Figure 3. Examples of the spatial distribution of the proportions of simulated particles following drift. (Left column shows proportions over regional bathymetry. Right column shows results at a larger scale, with bathymetric information suppressed. Closed areas are indicated by outlines.) These maps show the results of a two-week drift at the surface, in winter. The upper row illustrates a scenario with 3,691 particles released, while the lower row shows a scenario with the maximum number of particles: 59,834. The proportions presented in the two rows are very highly correlated ($r = 0.9956$).

Time Step

All correlations between sequential time steps greatly exceeded 0.90 (Figure 4). No strong spatial differences were seen between the results from scenarios using the different time steps (not shown). Although a longer, and so more economical, time step might have been used without loss of precision, we chose 60 min, a time step previously used by others (e.g. van Sebille et al. 2019), for subsequent model runs.

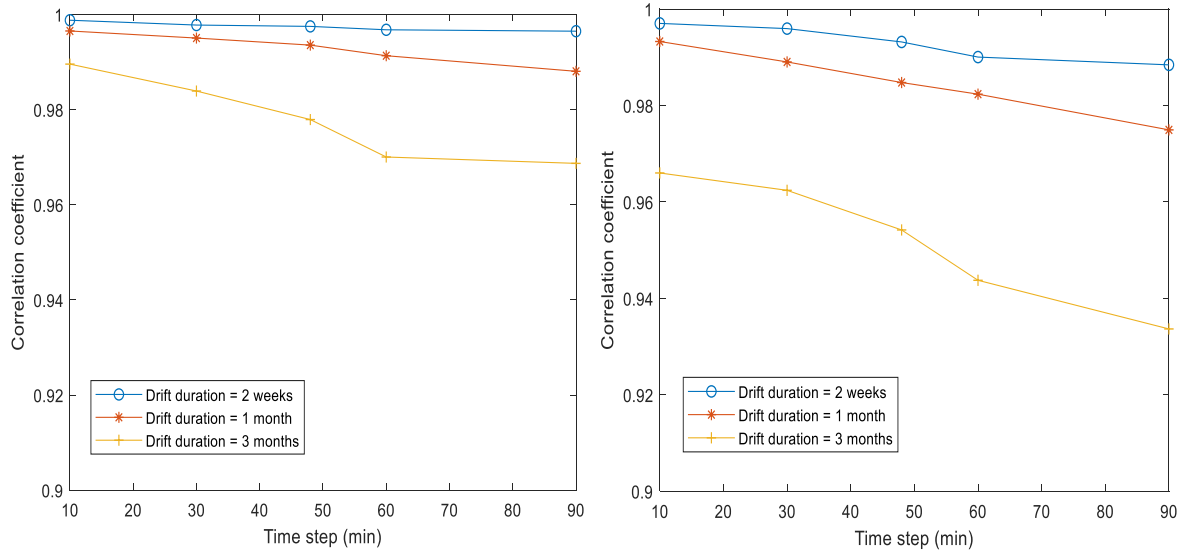


Figure 4. Correlation (r) between proportions of virtual particles in various grid cells, at the end of the drift duration, for sequential pairs of time steps (shorter time step in the pair is plotted) in winter scenarios at the surface (left) and at a depth of 100 m (right).

Random Walk

For each value of the diffusivity parameter, the correlation between results obtained with a random walk and those without was higher for the two-week drift duration than for the one month or three month durations. Indeed, the correlations for results after three months of drift were poor, the effect of random walk on the end position of the particles increasing with drift-duration. The correlations decreased gradually with increasing diffusivity but in most scenarios the rate of decline slowed with diffusivities above $100 \text{ m}^2 \text{ s}^{-1}$ (Figure 5; Table 3). The distributions of the particles at the end of each drift duration were generally similar among the scenarios, with the greatest contrast being between zero random walk and diffusivities of 100 or $200 \text{ m}^2 \text{ s}^{-1}$. The latter parameter values led to maps of particle distribution similar to one another, though those generated using $200 \text{ m}^2 \text{ s}^{-1}$ were more diffuse (Figures 6-11).

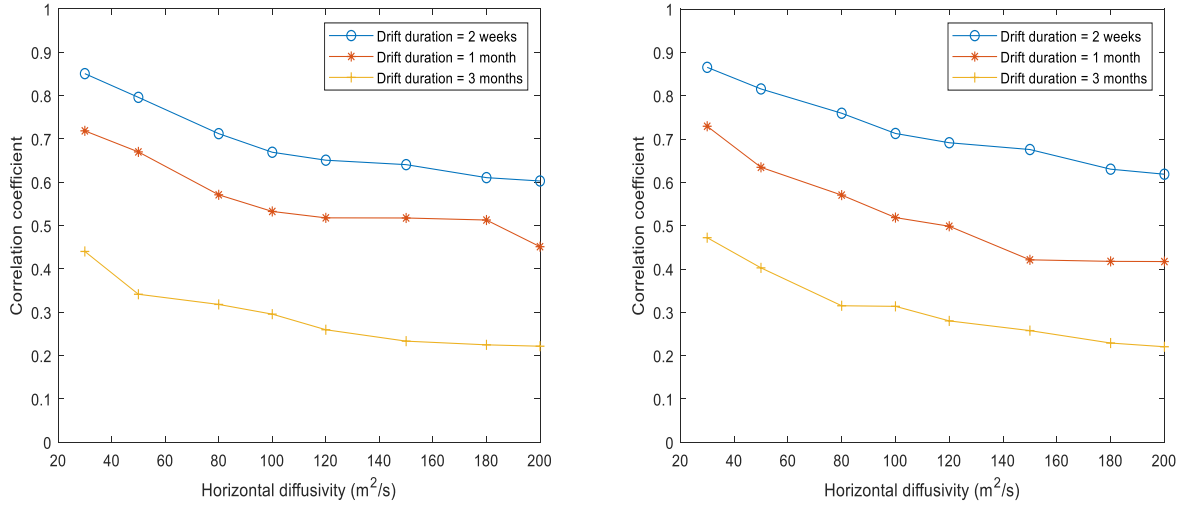


Figure 5. Correlation (r) between proportions of virtual particles in various grid cells, at the end of the drift duration, for scenarios with various values of horizontal diffusivity compared to a scenario with no Brownian movement, at the surface (left) and at a depth of 100 m (right), all calculated for the winter season.

Table 3. Correlations (r) between proportions of virtual particles in various grid cells, at the end of the drift duration, for selected scenarios with various values of horizontal diffusivity, calculated for the winter season.

Depth	Drift Duration	Correlation between No Random Walk and Horizontal Diffusivity Parameter Value	
		$100 \text{ m}^2 \text{ s}^{-1}$	$200 \text{ m}^2 \text{ s}^{-1}$
Surface	2 weeks	0.6693	0.6030
Surface	1 month	0.5327	0.4513
Surface	3months	0.2956	0.2216
100 m	2 weeks	0.7128	0.6188
100 m	1 month	0.5187	0.4172
100 m	3months	0.3138	0.2206

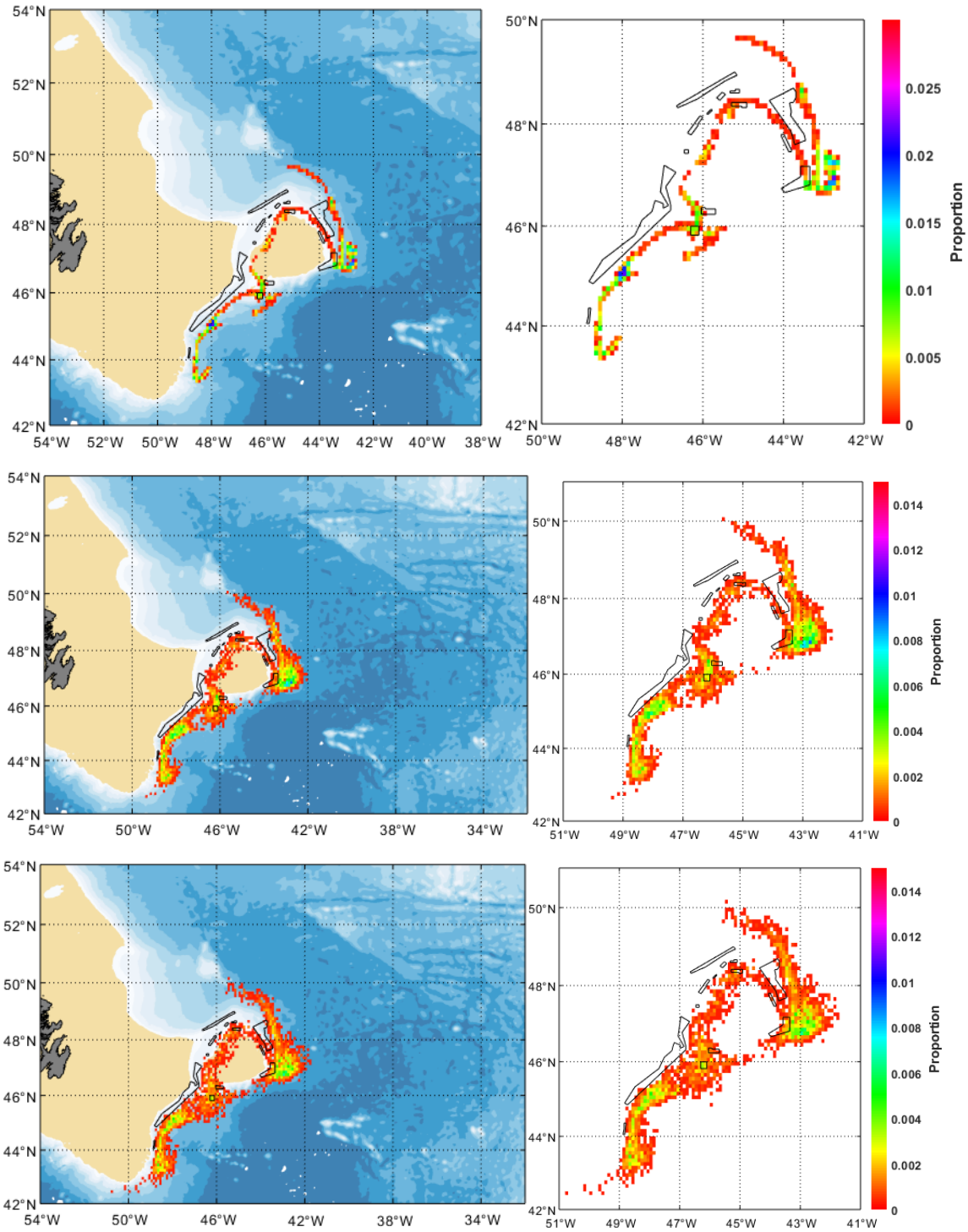


Figure 6. Spatial distributions of the proportions of simulated particles following a two-week drift duration at the surface, in winter. (Left column shows proportions over regional bathymetry. Right column shows results at a larger scale, with bathymetric information suppressed. Closed Areas are indicated by outlines.) Upper row: No random walk; Middle row: Horizontal diffusivity $100 \text{ m}^2 \text{ s}^{-1}$; Lower row: Horizontal diffusivity $200 \text{ m}^2 \text{ s}^{-1}$.

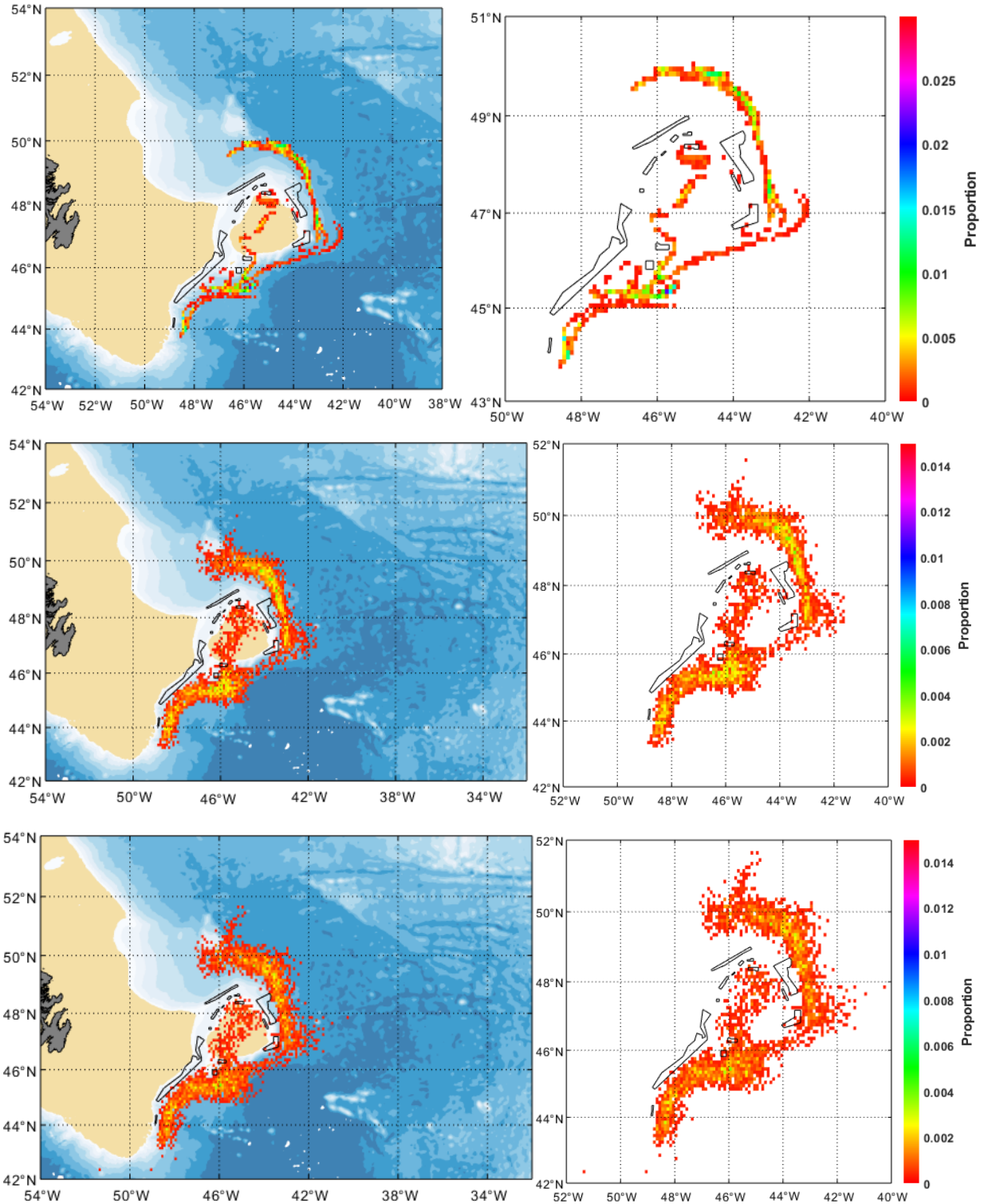


Figure 7. Spatial distributions of the proportions of simulated particles following a one-month drift duration at the surface, in winter. (Otherwise as Figure 6).

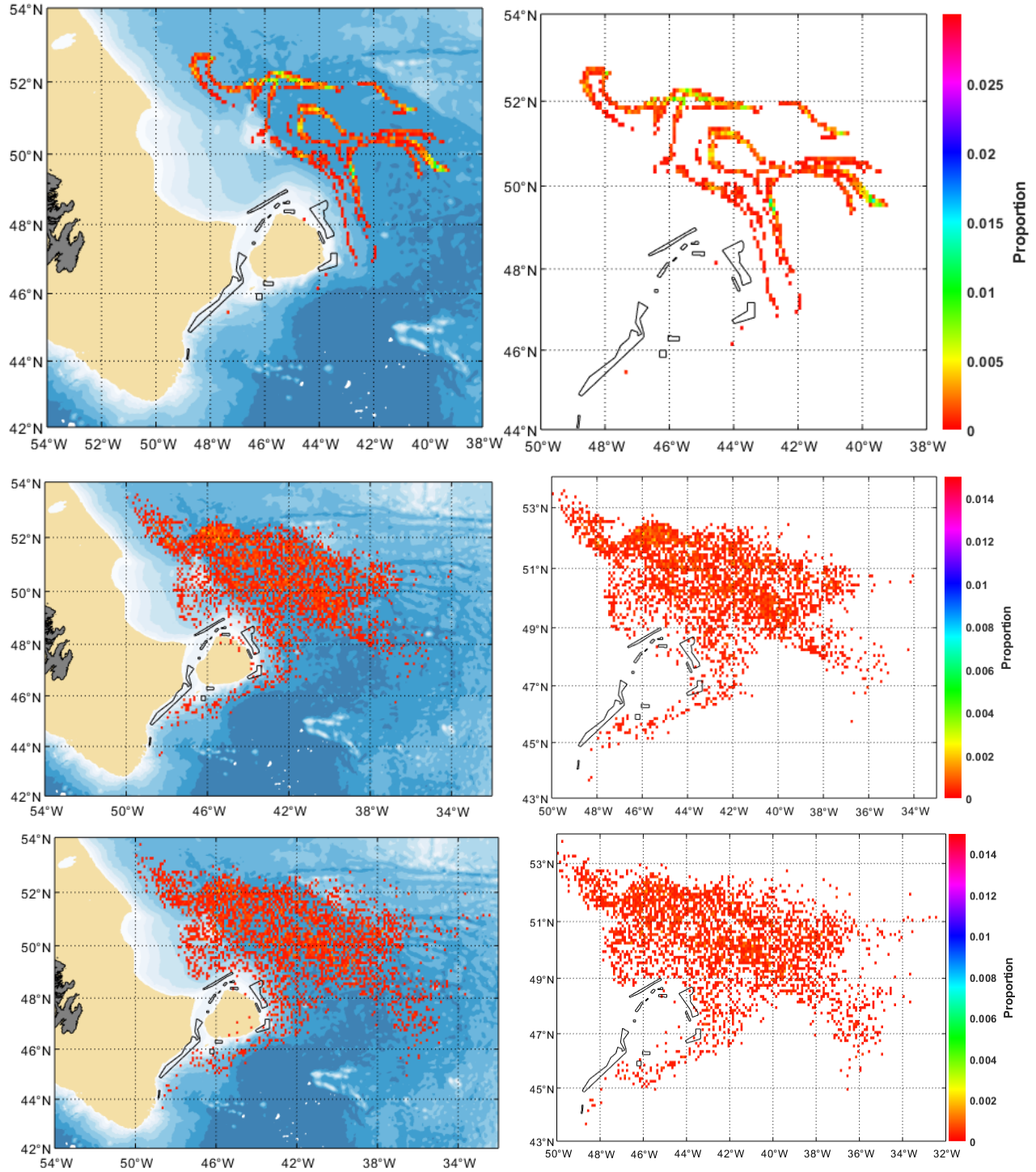


Figure 8. Spatial distributions of the proportions of simulated particles following a three-month drift duration at the surface, in winter. (Otherwise as Figure 6).

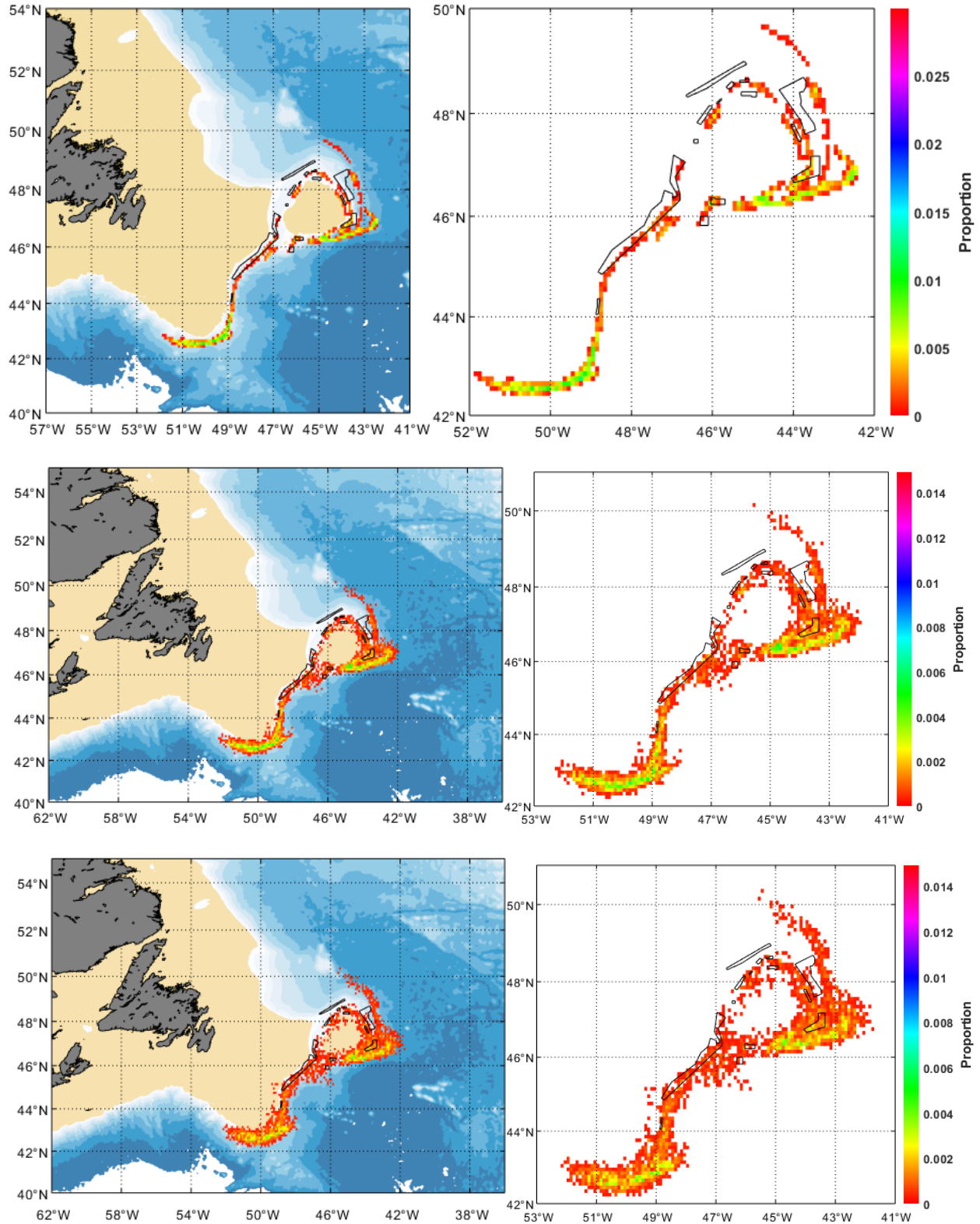


Figure 9. Spatial distributions of the proportions of simulated particles following a two-week drift duration at 100 m depth, in winter. (Otherwise as Figure 6).

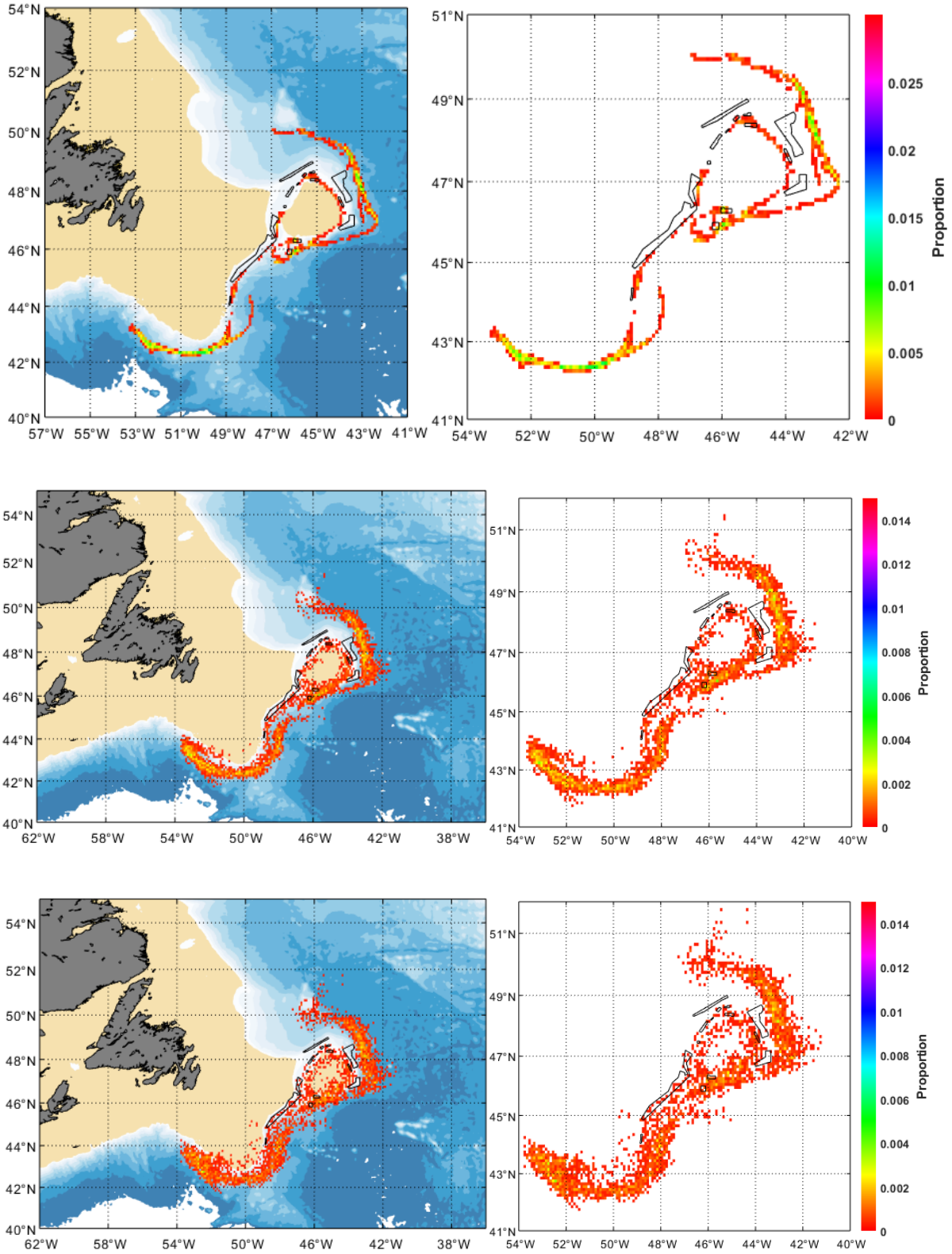


Figure 10. Spatial distributions of the proportions of simulated particles following a one-month drift duration at 100 m depth, in winter. (Otherwise as Figure 6).

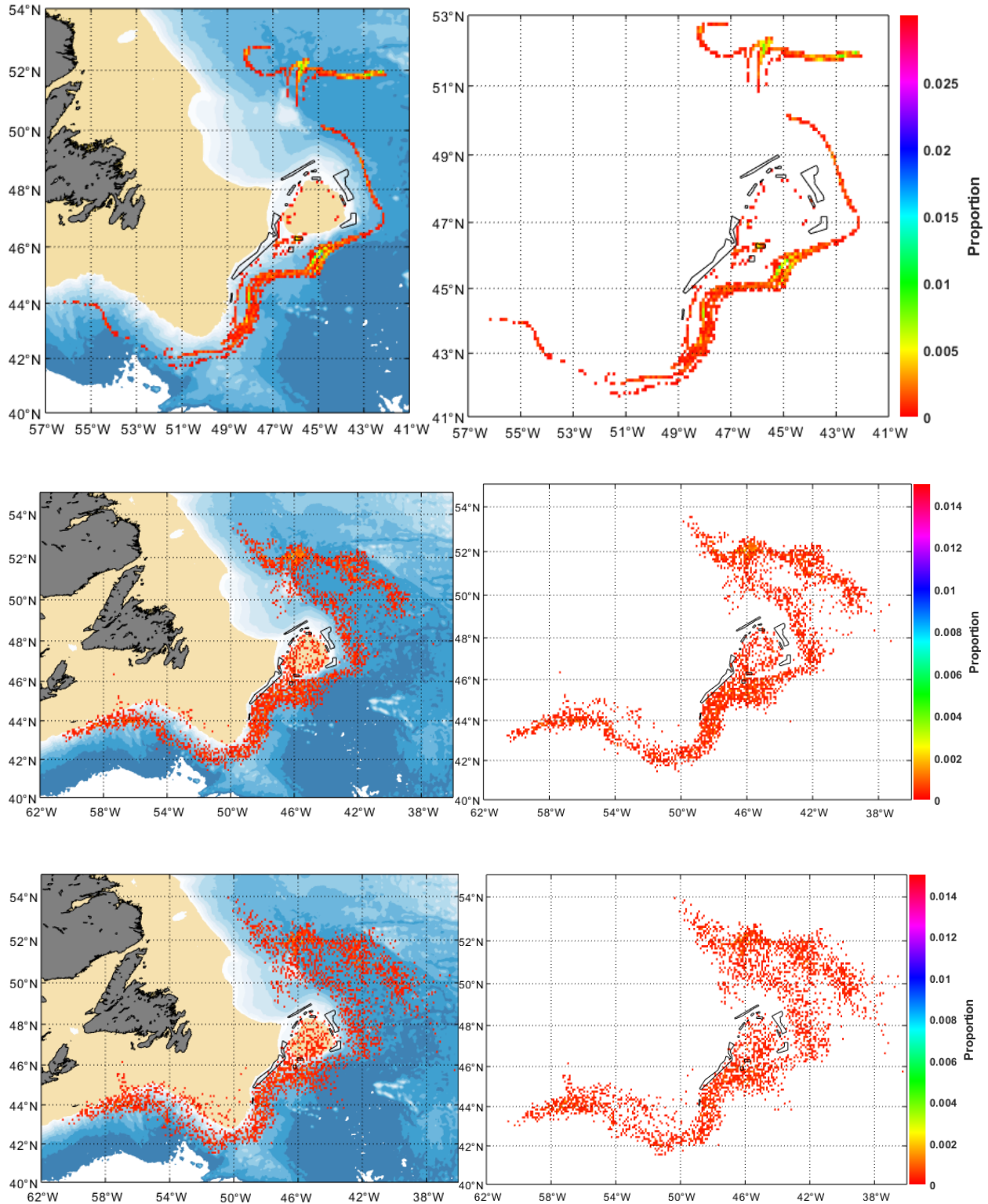


Figure 11. Spatial distributions of the proportions of simulated particles following a three-month drift duration at 100 m depth, in winter. (Otherwise as Figure 6).

Number of Particles with Random Walk Applied

With a horizontal diffusivity of $100 \text{ m}^2 \text{ s}^{-1}$, the correlation between proportions of virtual particles in various grid cells exceeded 0.9 and 0.8 respectively, after drift durations of one month and three months, when calculated for scenarios in which 14,909 and 18,404 particles were released. Larger numbers of particles had little further effect on the correlations after two-week and one-month drifts, while the correlations only increased slowly even after three-month durations (Figure 12). There were limited differences in the spatial distributions of the proportions of particles, at the end of each drift duration, between scenarios in which 3,691 (the optimal value without Brownian movement), 14,909 or 59,834 (the maximum number tested) particles were released (e.g., Figure 13). Thus, in subsequent model runs with Brownian movement (horizontal diffusivity $100 \text{ m}^2 \text{ s}^{-1}$), we released 14,909 particles at a particle spacing of 0.01° .

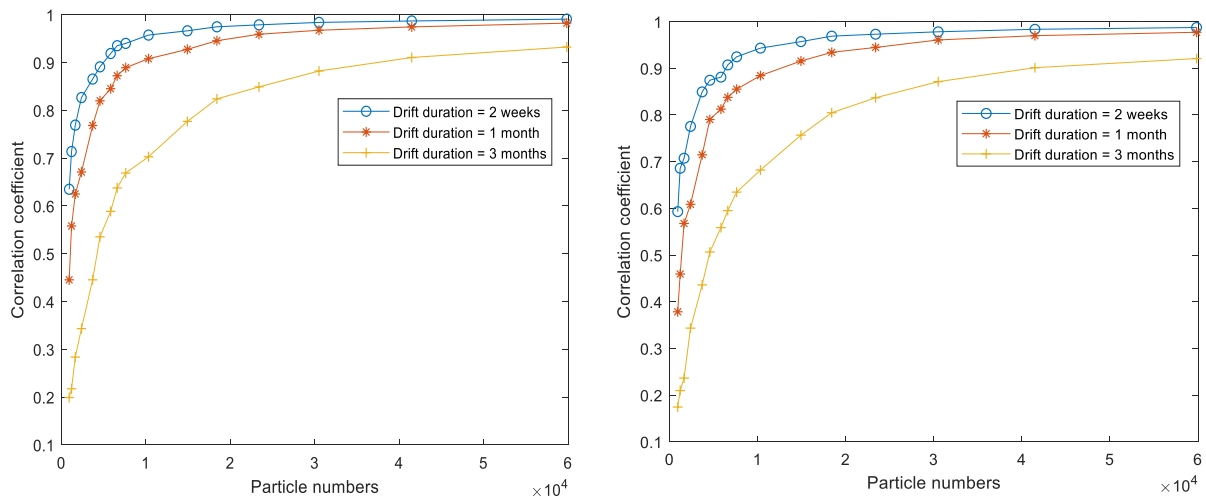


Figure 12. Correlation (r) between proportions of virtual particles in various grid cells, at the end of the drift duration, for sequential pairs of numbers of particles released in winter scenarios with horizontal diffusivity of $100 \text{ m}^2 \text{ s}^{-1}$ at the surface (left) and at a depth of 100 m (right).

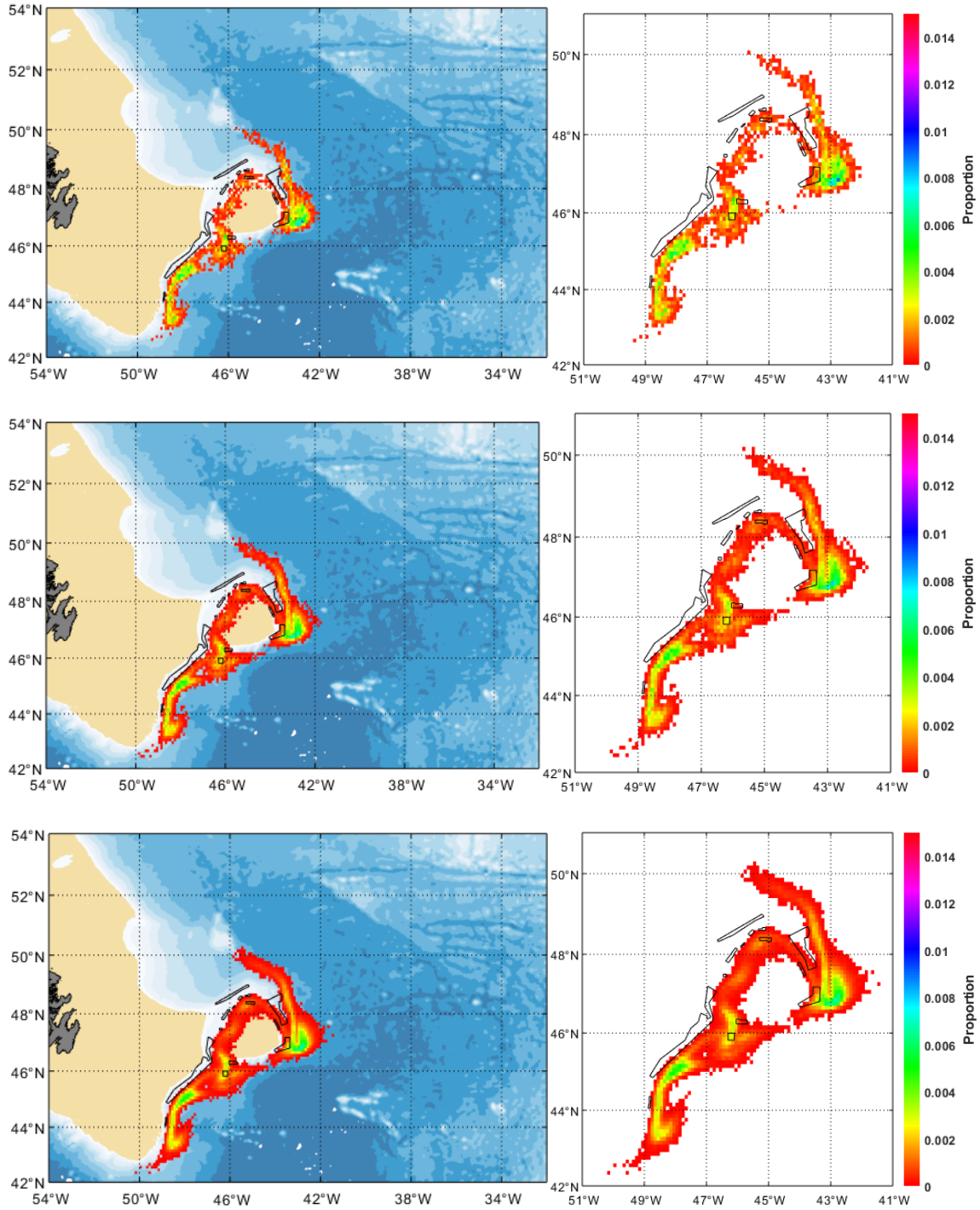


Figure 13. Examples of the spatial distribution of the proportions of simulated particles following drift. (Left column shows proportions over regional bathymetry. Right column shows results at a larger scale, with bathymetric information suppressed. Closed Areas are indicated by outlines.) These maps show the results of a two-week drift at the surface, in winter with horizontal diffusivity of $100 \text{ m}^2 \text{ s}^{-1}$. The upper row illustrates a scenario with 3,691 particles released, the middle row 14,909 and the lower row 59,834.

SIMULATION EXPERIMENTS

Impacts of Random Walk on Connectivity

Nine of the 14 closed areas have sufficient seabed depth for simulated particles to be released within them at 1000 m depth. Because only a single particle could be released within Closed Area 9, the comparisons for this area are not shown. Closed Area 1 is located generally down-current of the other areas and none of the particles released there passed over any other areas. The proportions of the particles released at 1000 m depth in each of the other seven closed areas that passed over each other area within each of the three drift durations, either with or without random walk, are shown in Figure 14. The introduction of random walk did not greatly change the connectivity amongst the closed areas, though there were quantitative differences in several cases. Most of those involved a lower number of drifts over another area, with less travel time (not shown), in the presence of random walk.

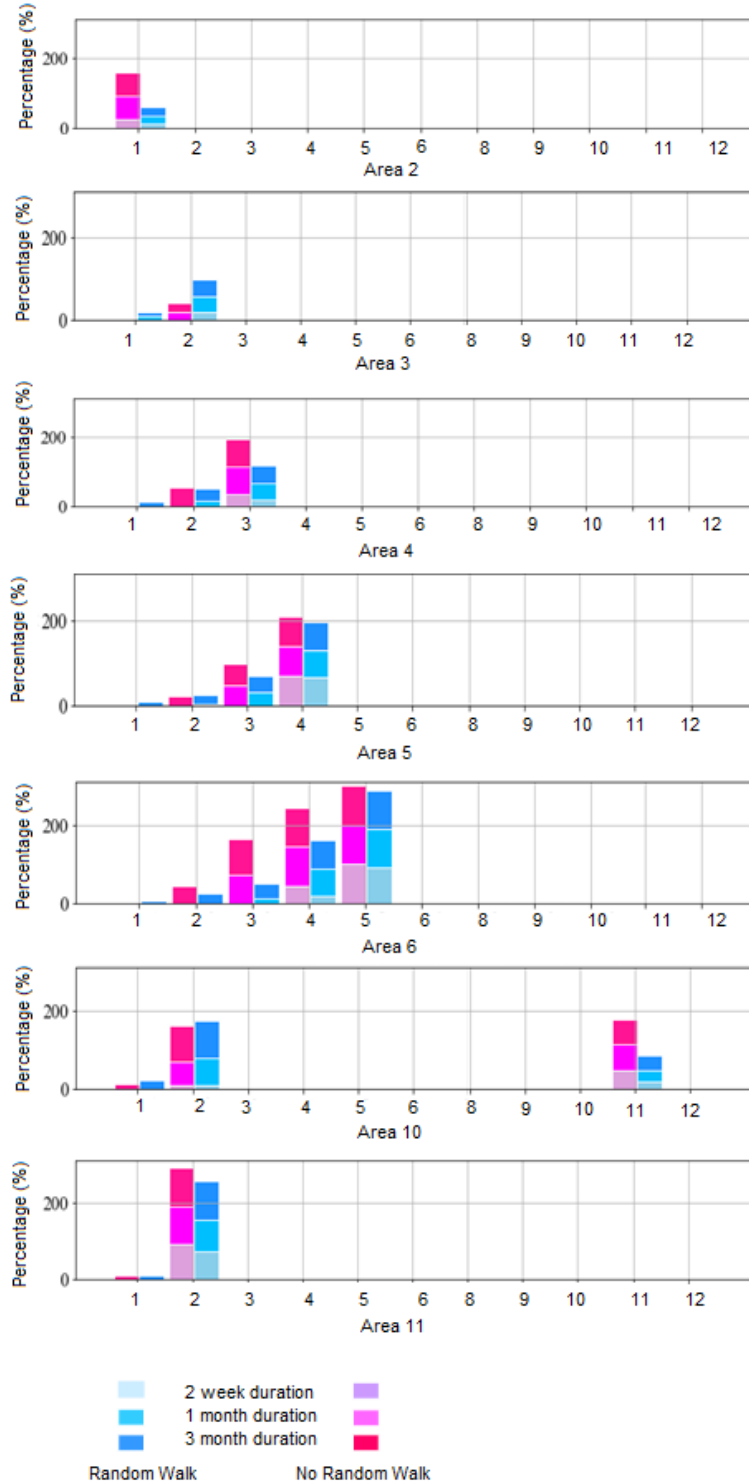


Figure 14. Percentages of particles, released at 1000 m depth in Closed Areas 2-6, 10 or 11, that passed over each other closed area during any of three drift durations (presented as cumulative histograms), generated by model runs with (reds) or without (blues) random walk. Note Areas 7, 13, and 14 are all shallower than 1000 m and so no connectivity is possible with 2-D models.

Identification of Potential Source Populations

Forward- and back-tracking of particle trajectories identified very similar potential source areas for larvae transported to the closed areas, though random walk introduced a stochastic component and so slight differences can be seen in the mapped results. The sources of two-week drifts at 1000 m depth were concentrated near the closed areas, particularly in Flemish Pass and westwards along the continental slope on the northern side of Grand Bank. Drifts at the surface or 100 m from that western area were more diffuse but showed a similar pattern (Figure 15). One-month drifts could also originate around Flemish Cap but more often came from the slope and outer continental shelf to the northwest, from where they would be carried to the closed areas by the Labrador Current (Figure 16). Some three-month drifts, particularly at 100 m depth, were retained locally. However, over that longest drift duration, the Close Areas could draw from source areas throughout the western side of the Labrador Sea (Figure 17).

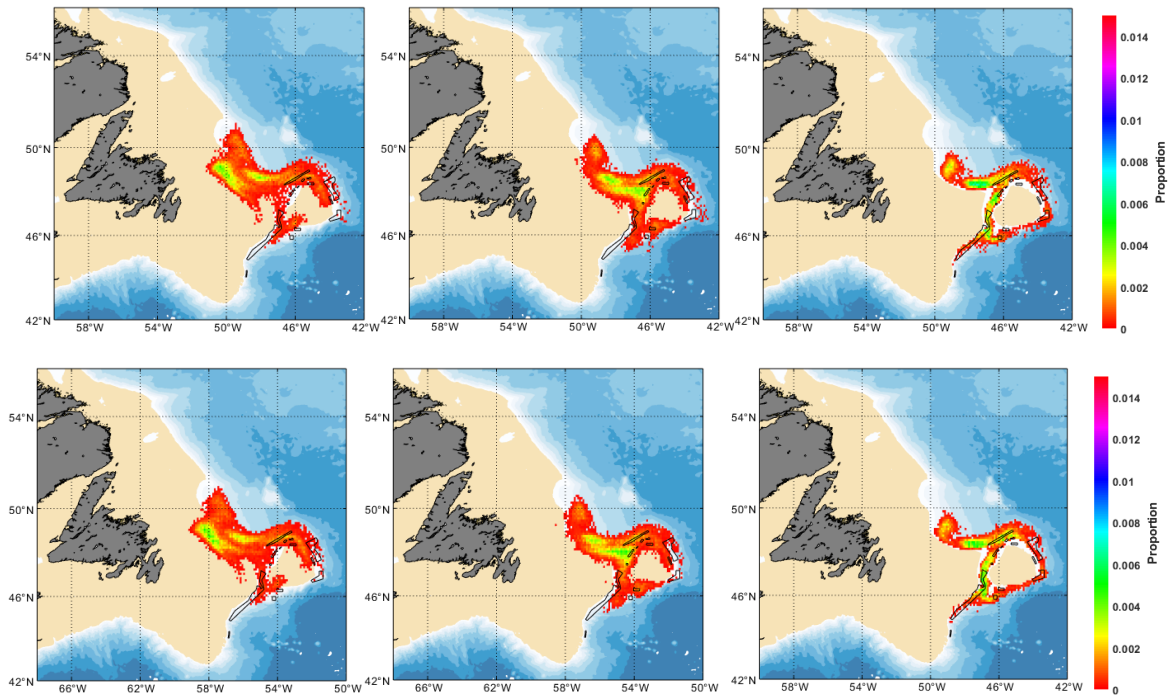


Figure 15. Spatial distribution of the sources of simulated particles which are in one of the closed areas after a two-week drift duration at (left) the surface, (middle) 100 m depth or (right) 1000 m depth, calculated by (upper) back-tracking and (lower) forward-tracking.

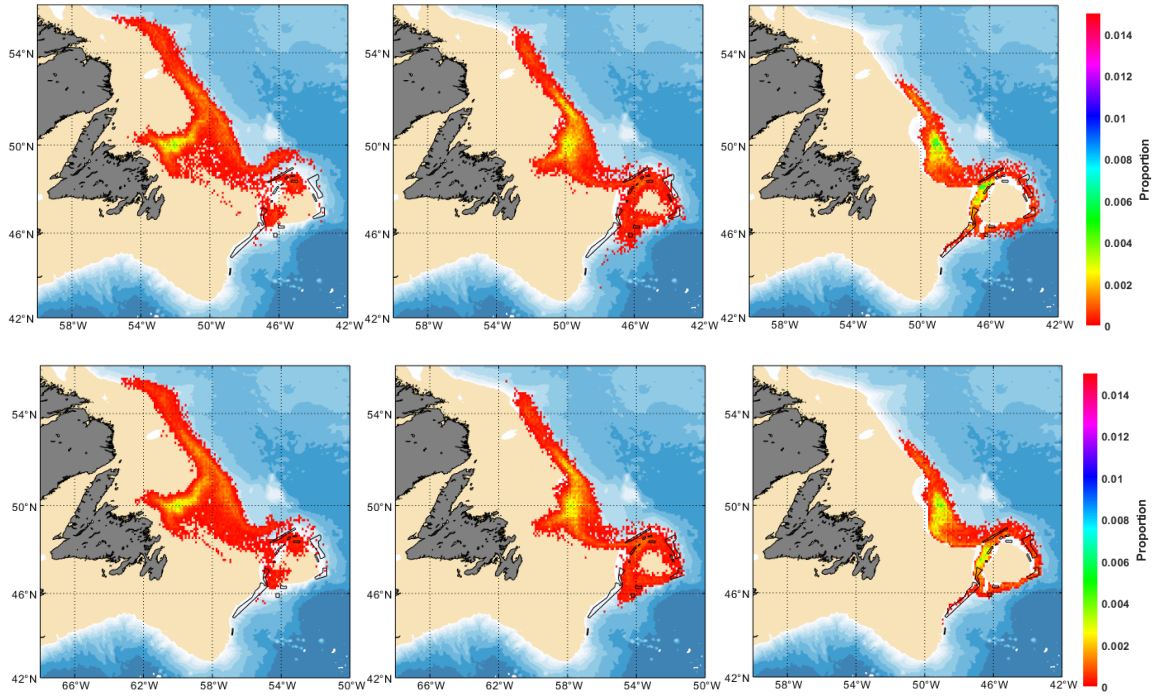


Figure 16. Spatial distribution of the sources of simulated particles which are in one of the closed areas after a one-month drift duration at (left) the surface, (middle) 100 m depth or (right) 1000 m depth, calculated by (upper) back-tracking and (lower) forward-tracking.

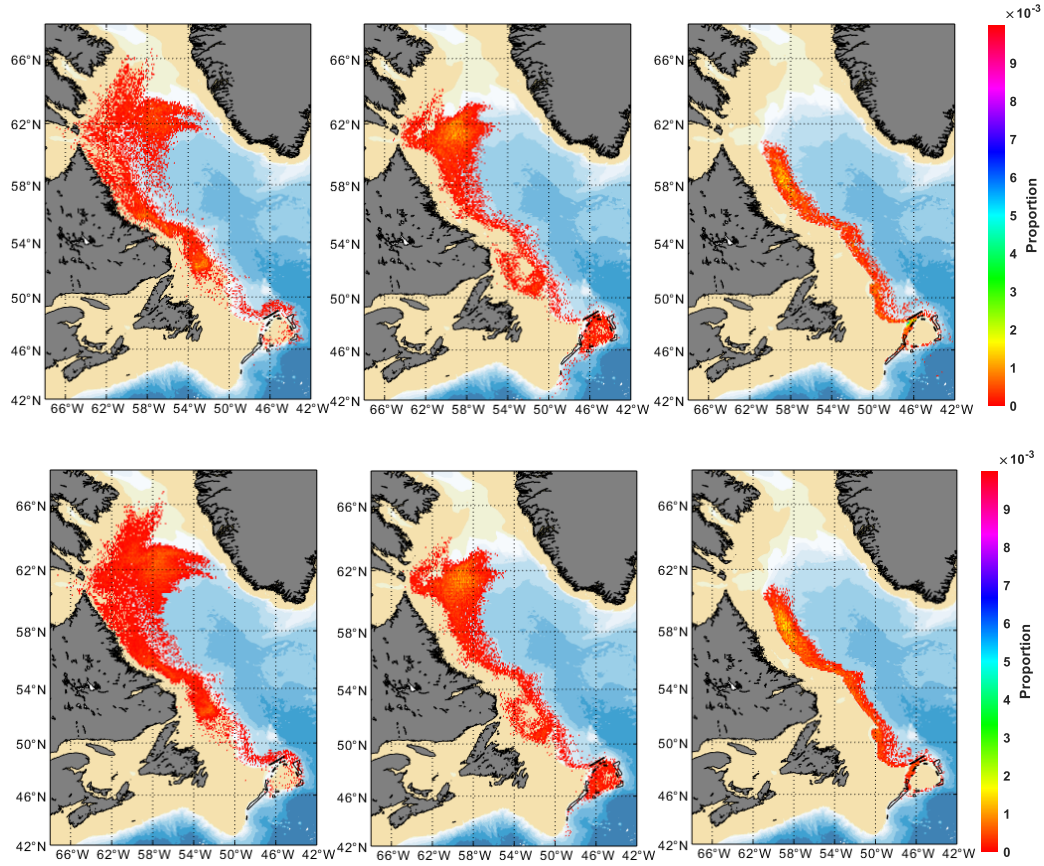


Figure 17. Spatial distribution of the sources of simulated particles which are in one of the closed areas after a three-month drift duration at (left) the surface, (middle) 100 m depth or (right) 1000 m depth, calculated by (upper) back-tracking and (lower) forward-tracking.

Connectivity Among Closed Areas

The magnitude of connectivity differed widely among pairs of closed areas (Tables 4–6, Figures 18, 19). Only one simulated particle released in Area 1 passed over any other closed area (not visible in Figure 19) and that took several weeks to reach Areas 2 and 3 (Figure 18; minimum=mean=maximum arrival time for this area).

Only a few particles from Area 2 reached any other closed area, most of them arriving in Area 1 (Figure 19). That connection could be swift, with a minimum transit time of 2 days at the surface or 100 m depth and 3 days at 1000 m (Figure 18). However, only 5% of particles released at the surface and 15% released at 100 m reached Area 1, which they did within two weeks. At 1000 m, 12% reached Area 1 within two weeks, 23% within a month and 25% within three months.

Few particles released in Area 3 reached any closed area other than Area 2 and that connection was only seen at 100 m and 1000 m depths (Tables 4-6, Figure 19). At 100 m, none reached Area

2 within two weeks but 17% did within one month and 34% within three months. At 1000 m, 18%, 39% and 41%, respectively, reached that area within the three drift durations.

Some particles released in Area 4 pass over Areas 13, 3, 2 and 1, with increasing drift times (Figure 19), and a high percentage of those released at 1000 m reached Area 3 eventually: 19% within two weeks, 49% within a month and 51% within two months. However, no particles released at the surface made that transit.

There was a close link from Area 5 to Area 4 with minimum arrival time of 2 days for all three depths (Figure 18), while the percentages of particles released in Area 5 that passed over Area 4 within two weeks were 44% at the surface, 63% at 100 m depth and 65% at 1000 m. Those percentages rose only slightly with longer drift durations.

The majority of particles released in Area 6 drifted clockwise around Flemish Cap, many crossing Areas 5 and 4, while some continue to Areas 3, 2 and 1. The connection from Area 6 to Area 5 was strong, with a minimum transit time of 3 days at the surface and 100 m depth or 5 days at 1000 m. Within two weeks, 70%, 86% and 91%, respectively, of the particles released at each of the three depths within Area 6 pass over Area 5.

Particles released at the surface in Area 7 also drifted clockwise around Flemish Cap, many passing across Areas 5, 14 or 4. Some of those released at 100 m moved through Flemish Pass into other Closed Areas.

Area 8 had connections with Areas 5 and 4 (Tables 4, 5). It took a minimum of 4 and 10 days, respectively, for particles released at the surface to reach those Areas (Figure 18). Within two weeks, 20% of those particles had entered Area 5 and 12% Area 4, percentages which increased to 21% and 62% within one month and to 22% and 88% within three months. There were similar connections at 100 m depth, though not as strongly with Area 4.

Particles released in Area 9 drifted clockwise around Flemish Cap, many passing over Areas 8, 7, 5 and 4. Of those released at the surface, some reached Area 7 in a minimum of 3 days (Figure 18), 44% passed over Area 7 within two weeks and 46% within one month (Figure 19), with no more entering thereafter.

Area 10 had strong connections through Flemish Pass with Area 11 and especially Area 2, though primarily at sub-surface depths. A very high proportion of particles released at 100 m or 1000 m in Area 10 reached some part of the large Area 2 (Figure 19) – at 100 m depth, 74% within two weeks, 90% within a month and 96% within three months. At 1000 m, the percentages were 10%, 68% and 98% respectively. While some particles took more than a month in transit, the minimum time was 5 days at 100 m and 9 days at 1000 m (Figure 18).

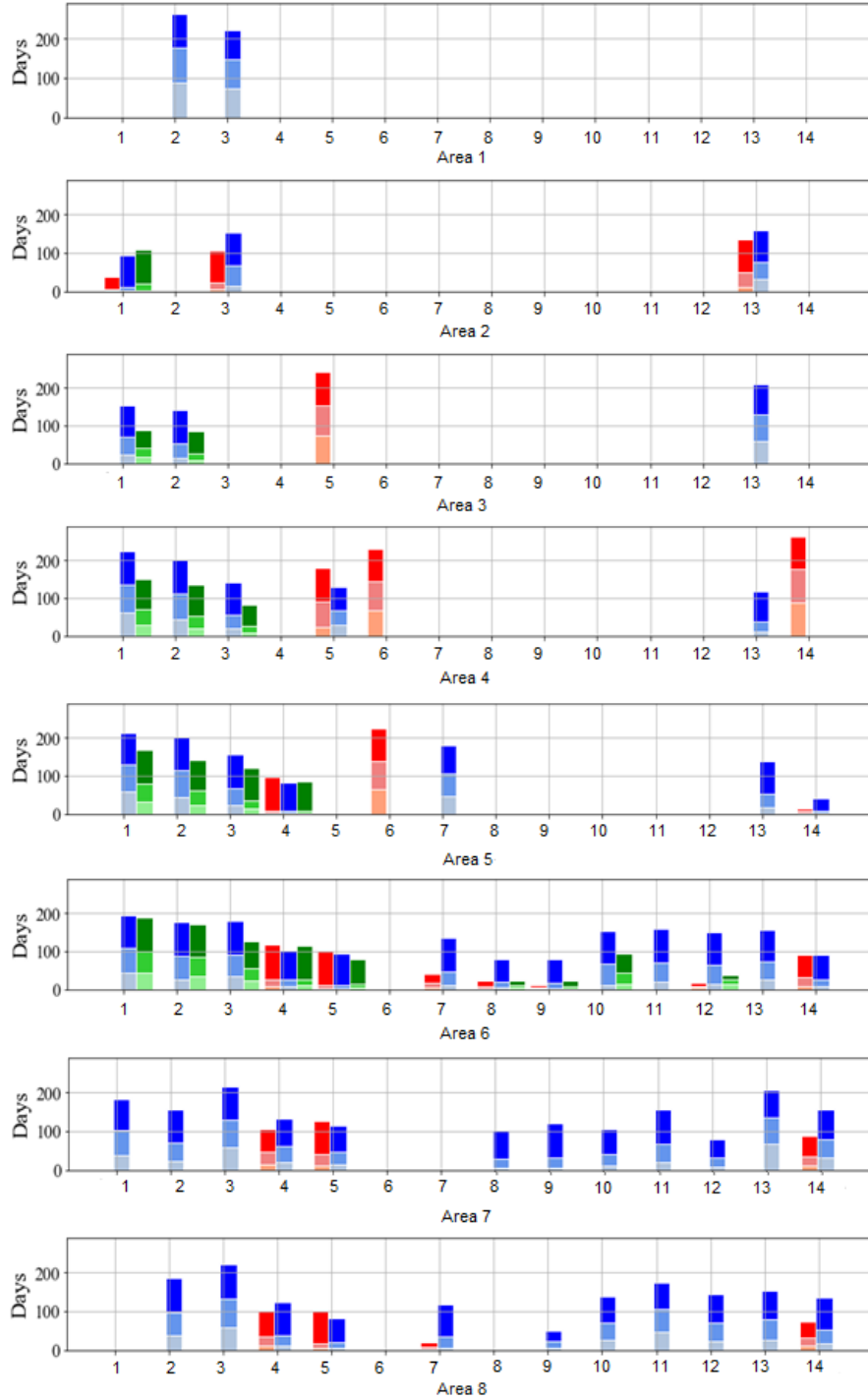


Figure 18. Results of the simulation experiments into connectivity between the closed areas, showing minimum, mean and maximum transit times between closed areas for simulated particles released in one closed area (Area X) that passed over another (numbered) and/or were retained in that Area by the end of the drift duration, with one histogram for each particle-release Area, and information on all 14 potential receiving Areas within each histogram. The results for particles released at the surface, 100 m and 1000 m depth are shown in adjacent, colour-coded columns.

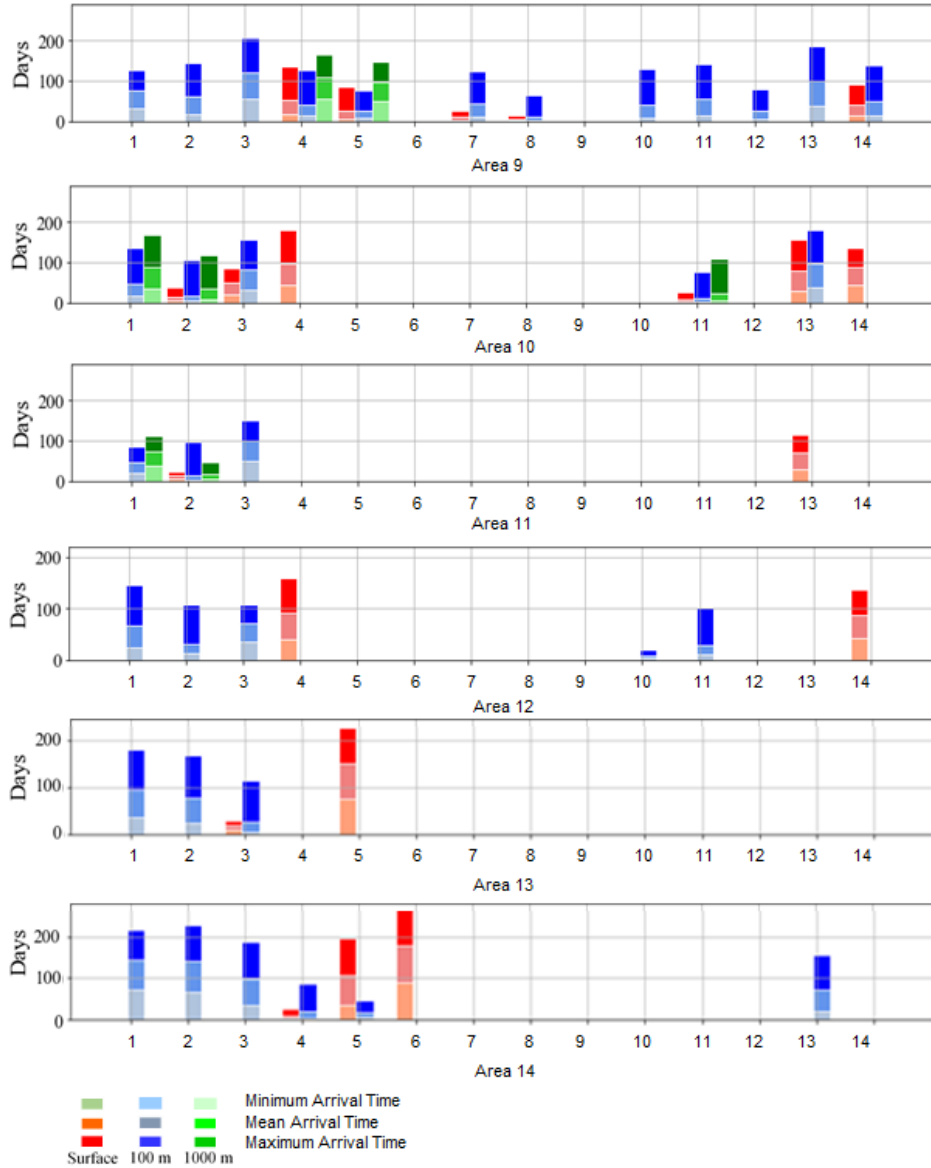


Figure 18 cont'd. Results of the simulation experiments into connectivity between the closed areas, showing minimum, mean and maximum transit times between closed areas for simulated particles released in one closed area (Area X) that passed over another (numbered) and/or were retained in that Area by the end of the drift duration, with one histogram for each particle-release Area, and information on all 14 potential receiving Areas within each histogram. The results for particles released at the surface, 100 m and 1000 m depth are shown in adjacent, colour-coded columns.

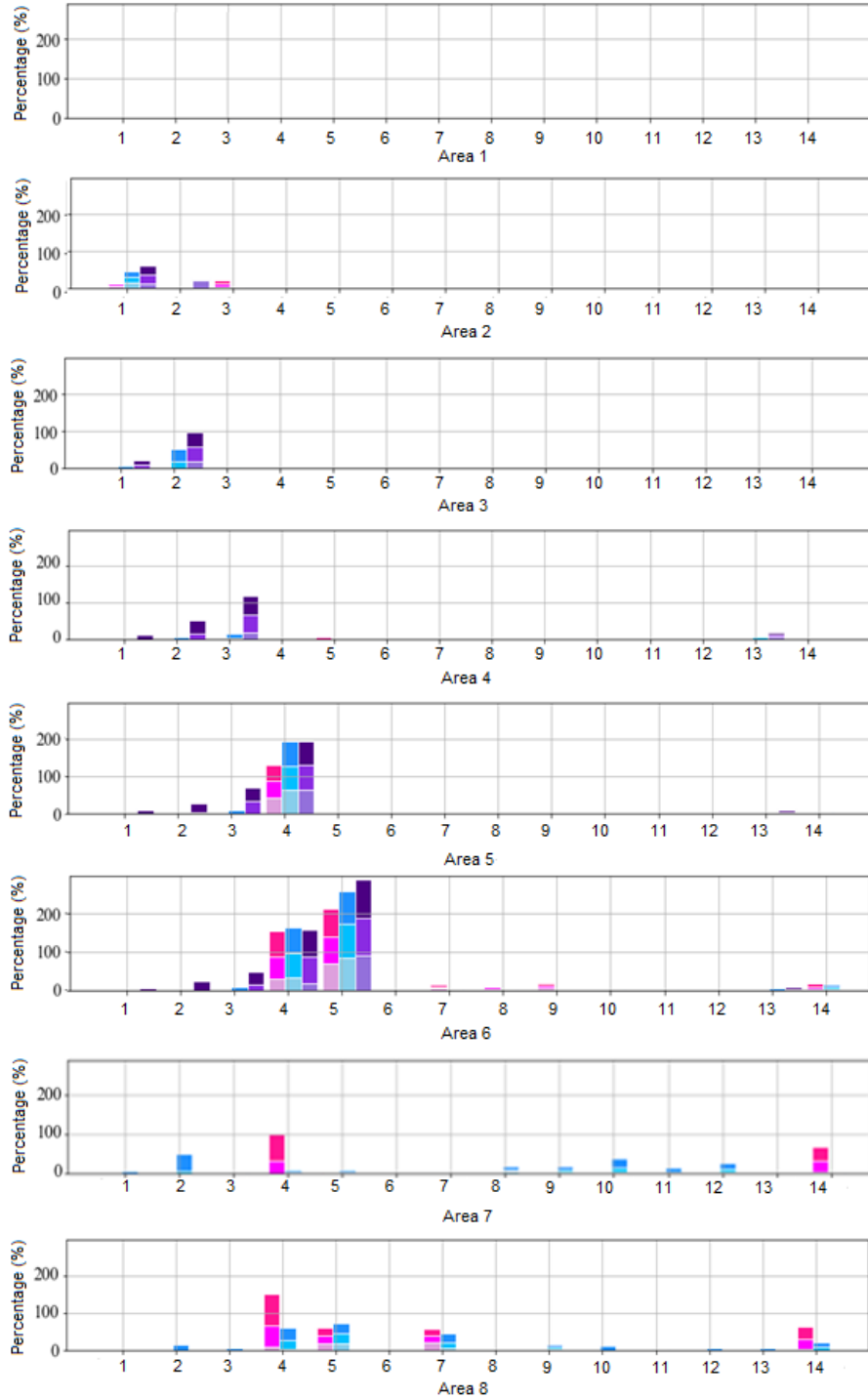


Figure 19. Results of the simulation experiments into connectivity between the closed areas, showing minimum, mean and maximum percentages of particles that passed over another closed area (numbered) and/or were retained in that Area by the end of the drift duration, with one histogram for each particle-release Area, and information on all 14 potential receiving Areas within each histogram. The results for particles released at the surface, 100 m and 1000 m depth are shown in adjacent, colour-coded columns.

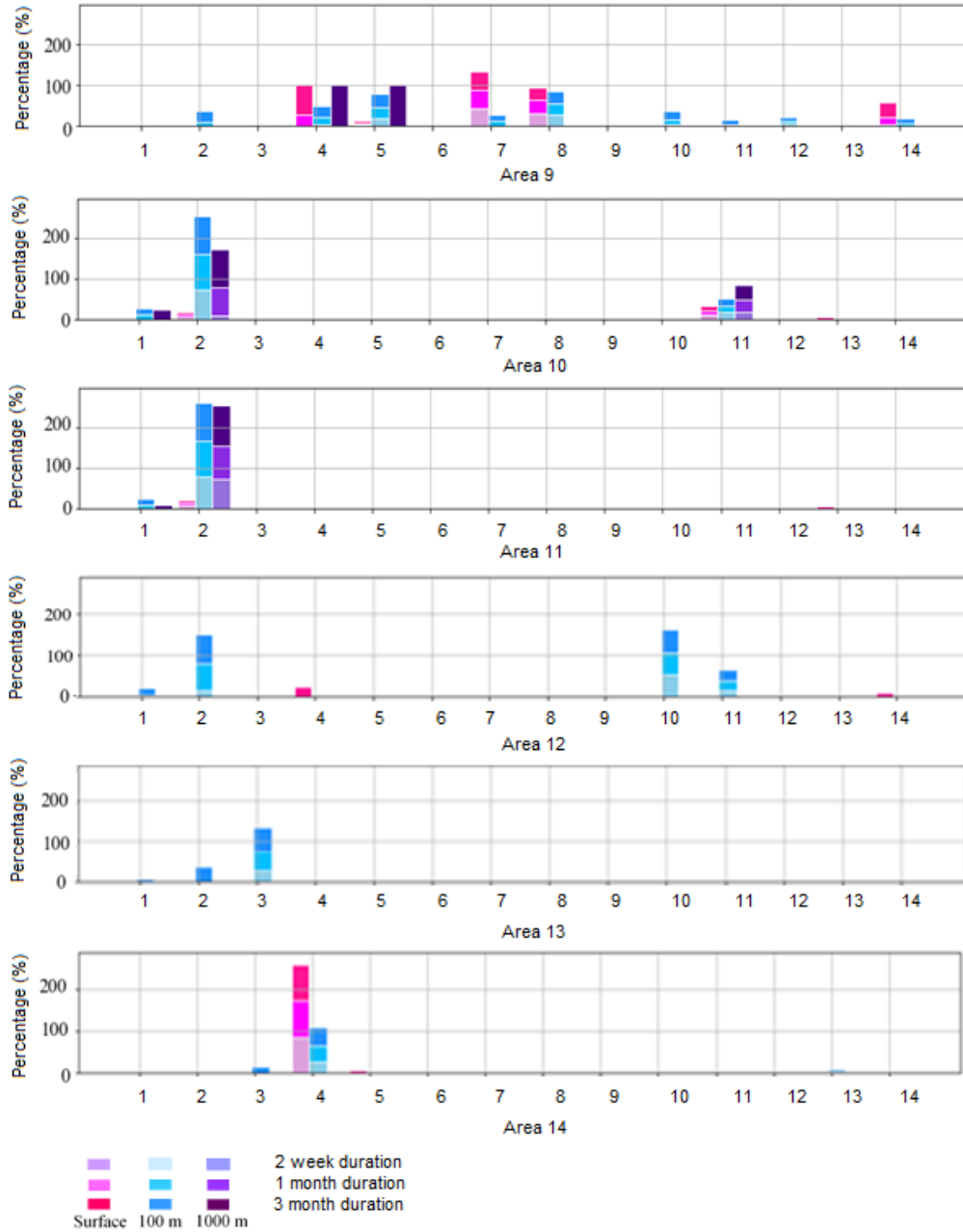


Figure 19 cont'd. Results of the simulation experiments into connectivity between the closed areas, showing minimum, mean and maximum percentages of particles that passed over another closed area (numbered) and/or were retained in that Area by the end of the drift duration, with one histogram for each particle-release Area, and information on all 14 potential receiving Areas within each histogram. The results for particles released at the surface, 100 m and 1000 m depth are shown in adjacent, colour-coded columns.

Nearly all particles released below the surface in Area 11 likewise passed over Area 2, 80% at 100 m and 73% at 1000 m within two weeks, those percentages rising to 89% and 82%, respectively, within one month and to 96% and 100% within three months.

Table 4. Connections between closed areas for modelled particle releases at the surface from within each closed area showing closed areas where particles first passed over (i.e., a connection made in a 2 week duration was not repeated for a 1 month duration although it would have passed over the area at 2 weeks of the 1 month time period) as well as those with endpoints within the release area (particle retention), by drift duration (2 weeks, 1 month, and 3 months).

Drift depth	Drift duration	Particles First Passing over/ Ending in Closed Areas from Release Area	Particle Endpoints within the Release Area
Surface	2 weeks	Area 2 to Areas 1, 3, 13	Areas 2, 4, 5, 7, 10
		Area 5 to Areas 4, 14	
		Area 6 to Areas 4, 5, 7, 8, 9, 12, 14	
		Area 7 to Areas 4, 5, 14	
		Area 8 to Areas 4, 5, 7, 14	
		Area 9 to Areas 5, 7, 8, 14	
		Area 10 to Areas 2, 11	
		Area 11 to Area 2	
		Area 13 to Area 3	
	Area 14 to Area 4		
	1 month	Area 4 to Area 5	Area 5
		Area 9 to Area 4	
Area 10 to Areas 3, 13			
3 months	Area 11 to Area 13	Areas 4, 5	
	Area 9 to Area 4		
	Area 3 to Area 5		
	Area 4 to Areas 6, 14		
	Area 5 to Area 6		
	Area 10 to Areas 4, 14		
	Area 12 to Areas 4, 14		
	Area 13 to Area 5		
	Area 14 to Area 5		

Few particles released at the surface in Area 12 passed over any other Closed Areas but many of those released at 100 m depth drifted through Flemish Pass, crossing Areas 10, 11, 2 or 1. The connection with Area 10 was strong, with a minimum transit time of 3 days and 66% of the particles entering that Area at some time within three months.

Very few particles released at the surface in Area 13 entered any other Closed Area but some released at 100 m depth eventually passed into either Areas 3, 2 or 1.

Table 5. Connections between closed areas for modelled particle releases at 100 m from within each closed area showing closed areas where particles first passed over as well as those with endpoints within the release area (particle retention), by drift duration (2 weeks, 1 month and 3 months).

Drift depth	Drift duration	Particles First Passing over/ Ending in Closed Areas from Release Area	Particle Endpoints within the Release Area
100 m	2 weeks	Area 2 to Areas 1, 3 Area 3 to Area 2 Area 4 to Area 13 Area 5 to Areas 4, 14 Area 6 to Areas 4, 5, 7, 8, 9, 10, 12, 14 Area 7 to Areas 5, 8, 9, 10, 12 Area 8 to Areas 4, 5, 7, 9 Area 9 to Areas 4, 5, 7, 8, 10, 12, 14 Area 10 to Areas 2, 11 Area 11 to Area 2 Area 12 to Areas 2, 10, 11 Area 13 to Area 3 Area 14 to Areas 4, 5	Areas 2, 5, 8, 9, 13, 14
	1 month	Area 3 to Area 1 Area 4 to Areas 3, 5 Area 5 to Areas 3, 13 Area 6 to Areas 2, 11, 13 Area 7 to Areas 2, 4, 11, 14 Area 8 to Areas 10, 12, 13, 14 Area 9 to Areas 2, 11 Area 10 to Area 1 Area 11 to Area 1 Area 12 to Area 1 Area 13 to Area 2 Area 14 to Area 13	Areas 2, 3, 4, 5, 7, 9, 13, 14
	3 months	Area 1 to Areas 2, 3 Area 2 to Area 13 Area 3 to Area 13 Area 4 to Areas 1, 2 Area 5 to Areas 1, 2, 7 Area 6 to Areas 1, 3 Area 7 to Areas 1, 3, 13 Area 8 to Areas 2, 3, 11 Area 9 to Areas 1, 3, 13 Area 10 to Areas 3, 13 Area 11 to Area 3 Area 12 to Area 3 Area 13 to Area 1 Area 14 to Areas 3, 2, 1	Areas 2, 3, 7, 13, 14

Table 6. Connections between closed areas for modelled particle releases at 1000 m from within each closed area showing closed areas where particles first passed over (i.e., a connection made in a 2 week duration was not repeated for a 1 month duration although it would have passed over the area at 2 weeks of the 1 month time period) as well as those with endpoints within the release area (particle retention), by drift duration (2 weeks, 1 month and 3 months).

Drift depth	Drift duration	Particles First Passing over/ Ending in Closed Areas from Release Area	Particle Endpoints within the Release Area
1000 m	2 weeks	Area 2 to Area 1	Areas 2, 10
		Area 3 to Area 2	
		Area 4 to Area 3	
		Area 5 to Areas 4, 3	
		Area 6 to Areas 4, 5, 8, 9, 10, 12	
		Area 10 to Areas 2, 11	
	1 month	Area 11 to Area 2	Area 2
		Area 3 to Area 1	
		Area 4 to Areas 1, 2	
3 months	Area 5 to Area 2	Area 2	
	Area 6 to Area 3		
	Area 5 to Area 1		
	Area 6 to Areas 1, 2		
	Area 9 to Areas 4, 5		
		Area 10 to Area 1	
		Area 11 to Area 1	

Many particles released at the surface in Area 14 pass over either Areas 4, or 5 (Table 4), with minimum transit times of 3, 35 and 90 days respectively. 87% of those particles enter Area 4 within two weeks but few others do so later. Many particles released at 100 m drifted clockwise around Flemish Cap, some passing over Areas 5, 4, 13, 3, 2 or 1. They could reach Area 4 with a minimum transit time of 3 days, 28% of them entering that Area within two weeks, 37% within a month and 46% within three months.

COMPARISON OF CONNECTIONS PRODUCED WITH WEBDROGUE AND PARCELS

Comparison of the endpoints of seasonally-modelled particle trajectories produced with Parcels and BNAM and those generated by Kenchington et al. (2019) with WebDrogue and the Quoddy ocean model showed no commonalities (Table 7). The comparison is limited to the number of particles with endpoints in another closed area as Kenchington et al. (2019) did not quantify particles passing over another closed area as detailed in the previous section. However, there were similarities of the trajectories along their lengths, even though the endpoints are different. For example in Table 7 the connection between Area 7 to Area 4 was not seen in surface drifts with

Table 7. Connections between closed areas for modelled particle releases from within each closed area with endpoints within another closed area, by season, drift depth, and drift duration in the water column. Connections made with WebDroque-modelled particle releases (Kenchington et al., 2019) are indicated in bold face.

Drift Depth	Drift Duration	Winter	Spring	Summer	Autumn
Surface	2 weeks	Area 2 to Area 3	Area 2 to Area 3	Area 6 to Area 4	Area 2 to Area 3
		Area 2 to Area 13	Area 6 to Area 4	Area 8 to Area 14	Area 6 to Area 4
		Area 6 to Area 4	Area 8 to Area 14		Area 6 to Area 7
		Area 6 to Area 5	Area 9 to Area 7		Area 9 to Area 7
		Area 8 to Area 4			
			Area 7 to Area 4		
	1 month	Area 9 to Area 4	Area 9 to Area 4	Area 6 to Area 4	
		Area 9 to Area 7	Area 9 to Area 14	Area 9 to Area 4	
	3 months	Area 9 to Area 4			
	100 m	2 weeks	Area 6 to Area 4		Area 8 to Area 5
Area 10 to Area 2					
Area 11 to Area 2					
Area 12 to Area 2					
Area 13 to Area 3					
			Area 9 to Area 8		
1 month		Area 7 to Area 2	Area 6 to Area 4	Area 6 to Area 4	Area 6 to Area 4
		Area 9 to Area 2	Area 10 to Area 2	Area 9 to Area 8	Area 6 to Area 5
		Area 14 to Area 7	Area 13 to Area 3	Area 10 to Area 2	Area 9 to Area 8
			Area 8 to Area 5	Area 11 to Area 2	Area 9 to Area 11
			Area 9 to Area 5	Area 10 to Area 2	
				Area 12 to Area 2	
				Area 4 to Area 14	
3 months			Area 8 to Area 7	Area 6 to Area 3	Area 9 to Area 2
			Area 8 to Area 14	Area 6 to Area 13	Area 11 to Area 2
			Area 9 to Area 14	Area 6 to Area 14	Area 12 to Area 2
			Area 12 to Area 2	Area 10 to Area 2	Area 7 to Area 3
			Area 7 to Area 5	Area 11 to Area 2	Area 13 to Area 3
			Area 9 to Area 5	Area 12 to Area 2	Area 14 to Area 2
			Area 12 to Area 7	Area 8 to Area 2	
			Area 9 to Area 2		
			Area 14 to Area 13		

Table 8. Connections between closed areas for modelled particle releases from within each closed area with endpoints within the same closed area (particle retention), by season, drift depth, and drift duration in the water column. Retention observed with WebDrogue-modelled particle releases (Kenchington et al. 2019) are indicated in bold face.

Drift depth	Drift duration	Winter	Spring	Summer	Autumn
Surface	2 weeks	Area 7			
	1 month				
	3 months				Area 5
100 m	2 weeks	Areas 2,13,14, 4	Areas 7, 2, 3, 4, 13	Areas 2,7,9,14	Areas 7, 13,14, 5
	1 month	Areas 13,14	Area 4	Areas 8, 9	Areas 9,14
	3 months	Areas 13,14, 4		Areas 8, 9	Area 14

Parcels, but Table 4 shows that particles released in Area 7 passed over Area 4. Similarly at 100 m particles released in Area 9 passed over Area 8 (Table 5) but did not end there (Table 7).

Across all seasons, the Parcels outputs showed much higher connectivity than that of WebDrogue. Retention was also higher and differed from that generated by WebDrogue, with higher retention found in the shallower closed areas with Parcels and BNAM (Table 8).

DISCUSSION

The complex nature of ocean currents makes replication of all their observed features by any model a challenge. In this Report, we have generated one set of simulations of connectivity among NAFO's 14 closed areas around Flemish Cap and the outer portion of Grand Bank, while mapping potential source areas for larvae that settle in those Areas – using the Parcels framework, with parameter values optimized for efficient use of computational time without compromising the outputs (specifically: 0.01° particle spacing, a 60 min time step and horizontal diffusivity of $100 \text{ m}^2 \text{ s}^{-1}$) and annual-mean currents. Those simulations generated a different impression from the seasonal simulations of Kenchington et al. (2019), based on WebDrogue, with generally higher degrees of connectivity among the closed areas and a broader swath of potential source areas. The observed difference will, in part, arise from the greater number of simulated particles seeded in the new scenarios, their foundation in annual-mean currents and their incorporation of random walk. However, much of the difference remained even when those factors were eliminated in seasonal Parcels runs, without random walk, that followed Kenchington et al. (2019) in the numbers of particles released.

Such differences between ocean models are not surprising. They can be present in many aspects of the models, including numerical methods, grid structure, resolution (horizontal and vertical) and

parameterizations of unresolved physical processes. Furthermore, the differences can lead to divergences in the presentation of oceanic quantities.

Parcels and WebDrogue both track particles based on the same kinematics formula:

$$x_t = \int_{t_0}^{t_1} v dt + x_0$$

Thus, in the 2-D simulations used here, any difference in the calculated position (x_t) for a given time (t) and release position (x_0) must be caused by differences in the velocities (v) imported from the ocean models (BNAM and Quoddy respectively). Due to unavailability of Quoddy results, we could not directly investigate the source of the differences between the models. However, inspection of simulated trajectories showed that many of the observed differences between the results of the two approaches can be explained by higher velocities in BNAM, which resulted in particle drifts calculated by Parcels following the same general tracks as those produced with WebDrogue and Quoddy but moving further.

BNAM and Quoddy belong to different families of ocean models. BNAM is a structured, z-level grid model (Madec et al. 2016). Models with a δ vertical grid, such as Quoddy, tend to overestimate vertical mixing for regions with large bathymetry gradients, which can negatively impact their representation of water properties and density structures in continental-slope areas. BNAM uses horizontally-structured grids, whereas Quoddy uses horizontally-unstructured grids. The unstructured grids have the advantage of depicting complex coast lines, which makes such models more suitable for simulating coastal waters but is less useful for areas far from land. Wang et al. (2019) have compared surface currents derived from BNAM with mapped currents derived from surface-drifter data, finding a strong correlation, which suggests that the model's outputs are realistic for the region of interest here. Thus, we suggest that the connectivity determined with Parcels should be considered to represent reality in the region around Flemish Cap better than did the results presented by Kenchington et al. (2019). Further, Parcels has the advantage of being able to simultaneously calculate the movements of a large number of particles in both 2-D and 3-D models. However, the complex currents in the region, particularly over the shallower portion of Flemish Cap, continue to pose a challenge for any connectivity study. Additional validation may be possible in the future.

Nor are any deficiencies in the physical modelling the major source of uncertainty. Knowledge of the seasonal and vertical distributions, as well as the drift durations, of the larvae of northwest Atlantic deep-sea sponges, sea pens and gorgonian corals remains very weak (Kenchington et al. 2019). Nothing is known of behaviours which may provide those larvae with some ability to enhance retention in their parental areas or to prolong their drifts if they encounter unsuitable seabeds when first ready to settle. Moreover, one of the characteristics which makes these benthic organisms highly vulnerable to anthropogenic stressors is that they have very high post-settlement life expectancies – even centuries for some corals. Thus, successful larval settlement, leading to recruitment of new colonies, may be a very rare event, occurring under atypical oceanographic

conditions. With such large biological uncertainty, physical models can usefully serve to scope plausible connectivity between areas but cannot conclusively demonstrate connections. The simulations generated here, using the Parcels framework, indicate that Parcels has the potential to fulfil the former function but 3-D models should be used to re-assess connectivity between the closed areas, rather than the 2-D models presented here used to compare with WebDrogue.

ACKNOWLEDGEMENTS

This project was supported by Fisheries and Oceans, Canada's International Governance Strategy (IGS) Research Fund, with funding to EK. Also, this research has been performed as a contribution to the SponGES project, which received funding from the European Union's Horizon 2020 research and innovation programme under grant agreement No. 679849. Dr. Shuangqiang Wang's contribution was funded through the Postdoctoral Research Program led by Natural Resources Canada, in collaboration with Fisheries and Oceans Canada. We thank Drs. Trevor Kenchington and F. Javier Murillo Perez (Fisheries & Oceans, Canada, Bedford Institute of Oceanography) for their careful review of this Report.

REFERENCES

- Adams, D. K., McGillicuddy, D. J., Zamudio, L., Thurnherr, A. M., Liang, X., Rouxel, O., German, C. R., and Mullineaux, L. 2011. Surface-generated mesoscale eddies transport deep-sea products from hydrothermal vents. *Science* 332(6029): 580–583. <https://doi.org/10.1126/science.1201066>
- Blanke, B., and Raynaud, S. 1997. Kinematics of the Pacific equatorial undercurrent: an Eulerian and Lagrangian approach from GCM results. *J. Phys. Oceanogr.* 27: 1038-1053.
- Blanton, B. 1995. DROG3-D: User's Manual for 3-Dimensional Drogue Tracking on a Finite Element Grid with Linear Finite Elements. University of North Carolina, Chapel Hill, North Carolina, U.S.A. 13 p.
- Bracco, A., Liu, G., Galaska, M., Quattrini, A. M., and Herrera, S. 2019. Integrating physical circulation models and genetic approaches to investigate population connectivity in deep-sea corals. *J. Marine Syst.* 198: 103189. <https://doi.org/10.1016/j.jmarsys.2019.103189>
- Breusing, C., Biastoch, A., Drews, A., Metaxas, A., Jollivet, D., Vrijenhoek, R.C., Bayer, T., Melzner, F., Sayavedra, L., Petersen, J.M., Dubilier, N., Schilhabel, M.B., Rosenstiel, P., and Reusch, T. B. H. 2016. Biophysical and population genetic models predict the presence of “phantom” stepping stones connecting mid-atlantic ridge vent ecosystems. *Curr. Biol.* 26: 2257–2267.

- Brickman, D., Hebert, D., and Wang, Z. 2018. Mechanism for the recent ocean warming events on the Scotian Shelf of eastern Canada. *Cont. Shelf Res.* 156: 11-22.
<https://doi.org/10.1016/j.csr.2018.01.001>
- Brickman, D., and Smith, P.C. 2002. Lagrangian stochastic modeling in coastal oceanography. *J Atmospheric Ocean. Technol.* 19: 83-99.
- Brickman, D., Wang, Z., and DeTracey, B. 2015. Variability of current streams in Atlantic Canadian waters: A model study. *Atmos. Ocean.* 54: 1-12.
<https://doi.org/10.1080/07055900.2015.1094026>
- Delandmeter, P., and van Sebille, E. 2019. The Parcels v2.0 Lagrangian framework: new field interpolation schemes. *Geosci. Model Dev.* 12: 3571–3584.
- Döös, K., Jönsson, B., and Kjellsson, J. 2017. Evaluation of oceanic and atmospheric trajectory schemes in the TRACMASS trajectory model v6.0. *Geosci. Model Dev.* 10: 1733-1749.
<https://doi.org/10.5194/gmd-10-1733-2017>
- Goldsmid, J., Nudds, S. H., Stewart, D. B., Higdon, J. W., Hannah, C. G., and Howland, K. L. 2019. Where else? Assessing zones of alternate ballast water exchange in the Canadian eastern Arctic. *Mar. Pollut. Bull.* 139: 74-90.
- Han, G., Lu, Z., Wang, Z., Helbig, J., Chen, N., de Young, B. 2008. Seasonal variability of the Labrador Current and shelf circulation off Newfoundland. *J. Geophys. Res.* 113: C10013.
<https://doi.org/10.1029/2007JC004376>
- Hannah, C. G., Shore J. A., and Loder, J. W. 2000. The retention-drift dichotomy on Browns Bank: a model study of interannual variability. *Can. J. Fish. Aquat. Sci.* 57: 2506-2518.
- Kenchington, E., Wang, Z., Lirette, C., Murillo, J. F., Guijarro, J., Yashayaev, I., and Maldonado, M. 2019. Connectivity modelling of areas closed to protect vulnerable marine ecosystems in the northwest Atlantic. *Deep-Sea Res. Pt. I* 143: 85–103.
<https://doi.org/10.1016/j.dsr.2018.11.007>
- Lange, M., and van Sebille, E. 2017. Parcels v0.9: prototyping a Lagrangian Ocean Analysis framework for the petascale age. *Geosci. Model Dev.* 10: 4175-4186.
- Luhar, A. K., and Rao, K. S. 1993. Random-walk model studies of the transport and diffusion of pollutants in katabatic flows. *Bound. -Layer Meteorol.* 66: 395-412.
- Lynch, D.R., and Werner, F.E. 1991. Three-Dimensional hydrodynamics on finite elements, Part II: Nonlinear time-stepping model. *Int. J. Numer. Methods Fluids* 12: 507-533.

- Madec, G., NEMO Team. 2016. NEMO Ocean Engine. Version 3.6 stable. Note du Pole de modélisation de l'Institut Pierre-Simon Laplace No 27. January 2016. 396 p. https://www.nemo-ocean.eu/wp-content/uploads/NEMO_book.pdf
- Van Sebille, E., Delandmeter, P., Schofield, J., Hardesty, B.D., Jones, J., and Donnelly, A. 2019. Basin-scale sources and pathways of microplastic that ends up in the Galápagos Archipelago. *Ocean Sci.* 15: 1341-1349.
- Wang, Z., Brickman, D., Greenan, B.J.W., and Yashayaev, I. 2016. An abrupt shift in the Labrador Current System in relation to winter NAO events. *J. Geophys. Res.* 121: 5338–5349. <https://doi.org/doi:10.1002/2016JC011721>
- Wang, Z., Brickman, D., and Greenan, B.J.W. 2019. Characteristic evolution of the Atlantic Meridional Overturning Circulation from 1990 to 2015: An eddy-resolving ocean model study. *Deep-Sea Res. Pt. I* 149: 103056. <https://doi.org/10.1016/j.dsr.2019.06.002>
- Werner, F., Page, F., Lynch, D., Loder, J., Lough, R., Perry, R., Greenberg, D., and Sinclair, M. 1993. Influence of mean advection and simple behavior on the distribution of cod and haddock early life stages on Georges Bank. *Fish. Oceanogr.* 2: 43-64.
- Xu, G., McGillicuddy, D. J., Jr., Mills, S. W., and Mullineaux, L. S. 2018. Dispersal of hydrothermal vent larvae at East Pacific Rise 9–10°N segment. *J. Geophys. Res.* 123: 7877–7895. <https://doi.org/10.1029/2018JC014290>
- Zeng, X., Adams, A., Roffer, M., and He, R. 2019. Potential connectivity among spatially distinct management zones for bonefish (*Albula vulpes*) via larval dispersal. *Environ. Biol. Fishes* 102: 233–252. <https://doi.org/10.1007/s10641-018-0826-z>

APPENDIX 1. CORRECTING PARTICLE TRAJECTORIES EXTENDING ONTO LAND THROUGH RANDOM WALK IN PARCELS

During runs of Parcels, calculated particle trajectories can extend onto land areas. That can occur when the time step is so large that particles step over multiple grid cells in one step or if random walk is implemented. It would be possible to solve the latter problem by writing a function to assess whether each particle is on land at each time step and, if so, making an appropriate correction. However, that would demand computational time. Alternatively, as particles move onto land because of non-zero horizontal diffusivity at the coast, setting the diffusion coefficient to zero on the land eliminates the problem.

That is easy to implement in Parcels by initializing the parameter with the following codes (for $100 \text{ m}^2 \text{ s}^{-1}$ of horizontal diffusivity):

```
from netCDF4 import Dataset

dataset = Dataset('mesh_mask.nc')

kh_zonal = dataset.variables['fmask'][:]

kh_meridional = dataset.variables['fmask'][:]

field_set.add_field(Field('Kh_zonal', kh_zonal*100, grid=field_set.U.grid))

field_set.add_field(Field('Kh_meridional', kh_meridional*100, grid=field_set.U.grid))
```

The ‘fmask’ variable saves a value of 0 or 1 for each grid node, as illustrated in Figure A1. When a particle moves near the land, the diffusion approaches zero by interpolation (though the spatial resolution is limited by the mesh dimension).

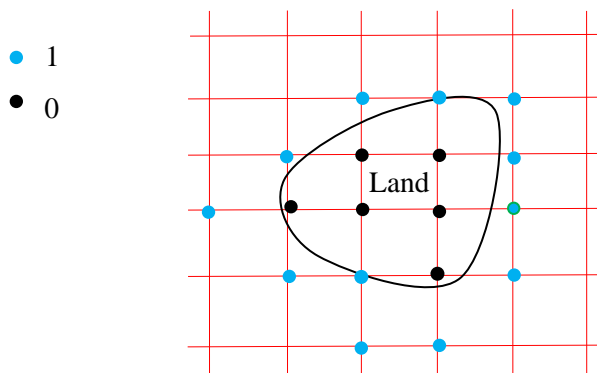


Figure A1. A schematic diagram to illustrate ‘fmask’. Black dots: Land nodes denoted by 0 in fmask file; Blue dots: Ocean nodes denoted by 1 in fmask file.